Large- and Small-Animal Studies of Safety, Pharmacokinetics (PK), and Biodistribution of Inflammasome-Targeting Nanoligomer in the Brain and Other Target Organs

Sydney Risen,[1] Breonna Kusick,[2] Sadhana Sharma,[3] Vincenzo S. Gilberto,[3] Stephen Brindley,[4] Mikayla Aguilar,[2] Jared M. Brown,[4] Stephanie McGrath,[2] Anushree Chatterjee,[3] Julie A. Moreno,[1,] Prashant Nagpal [3,*]*

[1] Environmental & Radiological Health Sciences and Brain Research Center, Colorado State University, Fort Collins, CO 80523

[2] Department of Clinical Sciences and Brain Research Center, College of Veterinary Medicine and Biomedical Sciences, Colorado State University, Fort Collins, CO 80523

[3] Sachi Bio, 685 S Arthur Avenue, Colorado Technology Center, Louisville, CO 80027

[4] Department of Pharmaceutical Sciences, University of Colorado Anschutz Medical Campus, Aurora, Colorado 80045

**Corresponding Authors. Email: nagpal@sachibio.com, julie.moreno@colostate.edu*

ABSTRACT:

The human immune system is the key line of defense in the body against infections and disease and is critical for our survival. However, immune malfunction or misrecognition of healthy cells and tissue, termed autoimmune disease, is implicated in more than 80 disease conditions and multiple other secondary pathologies. While pan-immunosuppressive therapies like steroids offer some relief for systemic inflammation for some organs, many patients never achieve remission and such drugs do not cross the blood-brain barrier making them ineffective for tackling neuroinflammation. Especially in the brain, unintended activation of microglia and astrocytes is hypothesized to be directly or indirectly responsible for several neurodegenerative diseases including Multiple Sclerosis (MS), Amyotrophic Lateral Sclerosis (ALS), Parkinson's Disease (PD), and Alzheimer's Disease (AD). Recent studies have also shown that targeting inflammasome and specific immune targets can be beneficial for a range of neurodegenerative diseases. Further, our previous studies have shown targeting NF-κB and NLRP3 through brain penetrant Nanoligomer cocktail SB_NI_112 (abbreviated to NI112) can be therapeutic for several neurodegenerative diseases. Here we show safety-toxicity studies, followed by pharmacokinetics (PK) and biodistribution in small- (mice) and large-animal (dog) studies of this inflammasome-targeting Nanoligomer cocktail NI 112 which downregulates NF-κB and NLRP3. We conducted studies using four different routes of administration: intravenous (IV), subcutaneous (SQ), intraperitoneal (IP), and intranasal (IN), and identified the drug concentration over time using inductively coupled plasma mass spectrometry (ICP-MS) in the blood serum, the brain (including different brain regions), and other target organs like liver, kidney, and colon. Our results indicate the Nanoligomer cocktail has a strong safety profile, has a consistent peak concentration in blood serum, and shows high biodistribution (F) and delivery across all routes of administration. Further analysis of multiexponential serum concentration with time shows while the bound/unbound ratio is highly dependent on the route of administration,

species (dog/mice), and dosage, the bound serum to Nanoligomer concentration in the brain is consistent at ~30%. Moreover, different dosing in dogs through IV and SQ routes also show predictability in bound serum concentration, and constant ratio when comparing large- and small-animal data (dog and mice). We hypothesize the constant ratio is determined by target protein amount, and PK parameters such as area under the curve (AUC) and can be used for more accurate interspecies scaling/dose determination. These results provide an excellent platform for translating and predicting therapeutic dosage between routes of administration in the same species, and a good prediction of scaling between species to attain similar target inhibition using high affinity and specificity of Nanoligomer binding the target.

KEYWORDS: Safety-Toxicity, Pharmacokinetics (PK), Biodistribution**,** Inflammasome-inhibitor, Nanoligomer, Antisense RNA therapeutic, large-animal dog studies.

INTRODUCTION:

Misrecognition of healthy cells, tissue, and organs by the immune system causes more than 80 chronic conditions and these autoimmune diseases affect more than 24 million people in the US alone, with rising prevalence.[1,2] Since these diseases disproportionality affect women, and are among the leading causes of death amongst young- and middle-aged women,[1,3] these diseases have an outsized impact on society and patients' families. Besides being directly implicated in neurological diseases related to motor function like Multiple Sclerosis (MS) and Amyotrophic Lateral Sclerosis (ALS), several other neurodegenerative diseases like Parkinson's Disease (PD) and Alzheimer's Disease (AD) are now hypothesized to be linked to non-specific microglial activation,[4–7] the resident immune cells in the brain. While there are no available cures for these autoimmune diseases and more specifically for neuroinflammation, pan-immunosuppressive steroids, and other non-specific therapies are utilized for managing symptoms and prolonging disease progression or symptom manifestation for systemic diseases. However, such non-specific immune suppressive methods have significant side effects, especially systemic effects while treating long-term chronic conditions.[8] Therefore, more targeted immune modulation[9,10] as well as detailed pharmacokinetic and route of administration studies are necessary for corticosteroids and pan-immunosuppressive therapies to manage adverse effects and contraindications.[8]

Specific Immune Targeting can Minimize Side-Effects

Selective inhibition of key inflammatory nodes/targets such as TNF, IL-17, IL-23, and IL-6 have improved the remission rates and replaced standard-of-care for a growing number of autoimmune diseases.[9,10] While recent advances in even more target-specific therapies such as tyrosine kinase 2 (TYK2) instead of Janus kinase (JAK) inhibitors offer further hope in reducing side-effects (e.g. abnormal changes in blood cell, cholesterol, triglyceride levels, etc.),[11] use of more traditional pharmaceutical modalities such as small-molecule-based targeting is slow and low-throughput with mixed safety profile. On the other hand, high-throughput approaches such as design-based antisense oligonucleotides (ASOs)[12] can potentially improve translation rates, but suffer from delivery challenges, especially for neurological diseases,[13,14] and accumulation in first-pass organs.[15,16] The emergence of new RNA-targeting antisense modalities such as

Nanoligomers can have the combined advantage of high delivery and biodistribution profile of small molecules, extremely high target-binding affinity (K_D ~3-5 nM) like antibodies, with the specificity and ease of design using nucleic acid-targeting.[17–23] Nanoligomers are peptide nucleic-acid-based RNA therapeutic modality that have shown targeted up-and down-regulation of proteins, with extremely high specificity, minimal off-targets, and a high safety profile.[17–23] However, more detailed safety-toxicity and biodistribution studies need to be conducted across small- and large-animal models for these new modalities to gain greater acceptance towards human clinical translation and pharma adoption.

Small- and Large-Animal Studies for Safety and Biodistribution and Intraspecies Scaling

While rodents are acceptable small-animal models for autoimmune and neurological disease modeling and induction, dogs are the preferred large-animal model for clinical drug translation to further assess the safety profile, central nervous system (CNS) pharmacokinetic (PK)/pharmacodynamic (PD), and biodistribution parameters.[24] We conducted extensive small- and large-animal studies for our targeted inflammasome inhibitor, an NF-κB and NLRP3 inhibitor combination (herein described as SB_NI_112 or NI112 in short) as the active pharmaceutical ingredient (API),[17–22] to assess safety-toxicity, develop a PK and biodistribution model to obtain relevant pharmacological parameters, and obtain insights for interspecies scaling for further translation. We observed extremely high biodistribution parameters across different routes of administration (biodistribution parameter F >0.98), excellent drug delivery across the blood-brain barrier (BBB) (brain tissue concentration ≥ 25-30% of blood serum bound concentration), rapid absorption across different brain sections, lack of accumulation in first-pass organs, as well as renal clearance of unbound/excess drug (or missense molecules).[19,20] These pharmacological results prove the potential for further translation and the need for the adoption of new therapeutic modalities for the benefit of millions of patients across multiple autoimmune and CNS diseases.

RESULTS AND DISCUSSION:

We utilized four different routes of administration: intravenous (IV), subcutaneous (SQ), intraperitoneal (IP), and intranasal (IN) for a comprehensive assessment of safety-toxicity and biodistribution profile in both small-animal (C57BL/6 mice) and large-animal (beagle dog) models. We explored dose-scaling in different routes, biodistribution parameters, and interspecies scaling, reported in this work.

Safety-Toxicity Assessment: Long-Term Repeat Dosing, 14-day Acute (5x MTD) Dosing in Small- and Large-Animals for CNS

We first started with a maximum tolerable dose (MTD) assessment of the NF-κB and NLRP3 inhibitor combination NI112. Prior studies have shown assessment of NI112 in relevant disease models,[17,18,22,23] and Nanoligomer selectivity and high-binding affinity (K_D 3.17 nM,[19,20] other PNA/RNA and PNA/DNA binding studies showed K_D 5-8 nM[25]) along with rapid biodistribution and clearance. We observed strong safety-toxicity profile in both animal models for longer-term repeat dosing (IP, 150 mg/kg, 3x a week for 12 weeks, **Fig. 1A**, **B, S1, S2**) as well as single-dose acute toxicity (5x maximum tolerable dose or MTD for IV) followed by 14-

day toxicity assessment and clinical monitoring (**Fig. S3, 1C-F, S4, S5)**. An important finding was that a single route (IV) showed a measurable MTD (100 mg/kg in mice, between 15-65 mg/kg in dogs), while other routes showed values well over 450-500 mg/kg, beyond the limit of testing parameters due to solubility limits. As shown in MTD **Table I** below and **Fig. S3,** the use of missense Nanoligomers (dog NI112 in mice) also showed no tolerability issues for 450-500 mg/kg IV. IV route demonstrates extremely rapid delivery and uptake of Nanoligomers in the brain and other organs (~ minutes), and some test subjects showed some adverse events (AEs) at high concentrations (75 mg/kg in dogs, **Fig. S3**). However, the PK and biodistribution of other routes are slightly slower, leading to better tolerance for high drug-dosing. This along with lack of such MTD for missense administration suggests that the AEs are related to the speed/rapid uptake and target inhibition in the brain and other organs, rather than potential side-effects of the API/drug. The lack of such threshold for missense Nanoligomer also suggests the specificity of target engagement by the drug. We note during dog studies, one subject animal showed acute injection site pain, swelling, and discomfort at 75 mg/kg SQ dosing, which was traced back to the high pH of SQ injection[26] due to the use of unbuffered saline media to dissolve dried NI112 powder. However, all subsequent dosing used phosphate-buffered saline (PBS), and no animal showed any issues with site injection pain or swelling.

Table I: MTD measurements for Mice and Dog Studies Using IV and SQ route of Administration

n=4 for mice studies, n=1-3 for dog studies. 1-test subject each in mice and dog studies showed side-effect/tolerability limit with the IV route, the mouse had experienced seizure-like behavior and the dog exhibited excess salivation and vomiting.

Admin Route	Molecule	Species	MTD (mg/kg)
IV	NI112_Mouse	Mouse	100
SQ			>450
IV	NI112_Dog (Missense)	Mouse	>450
SQ			>450
IV	NI112_Dog	Dog	15
SQ			>67.5

Using these MTD values, we conducted two types of repeat-dosing (using IP) and acute-dosing tests (using IV and SQ). Due to rapid aging in mice, we used 13–15-week-old mice for longer-term (12-week) repeat dosing (3x a week, for chronic diseases) with IP injections, to assess any biochemical or histological changes compared to sham-treated control animals. As shown in **Fig. 1A**, we conducted a detailed blood serum evaluation using 36-cytokine and chemokine biomarkers in blood, for any potential immunological or adverse outcomes (through clinical/health monitoring). We did not observe any statistical change (detailed p-values shown in **Fig. S1**) in any biomarker. Further, we conducted a detailed histological evaluation and scoring for the first pass and clearance organs (liver, kidney, colon, **Fig. 1B, S2**) for chronic-dosed

animals, essential for drug metabolism and excretion. We did not observe any evidence of accumulation, organ damage, toxicity, or any immune cell infiltration, as shown using H&E staining. Also, in long-term studies, there was no evidence of accumulation or resulting inflammation in the medulla or nephrons (within glomeruli, **Fig. 1B**), supporting renal clearance for Nanoligomer molecules.[19,20] These results again demonstrate the high safety profile of the drug for repeat dosing over longer periods.

Next, we conducted acute dose toxicity monitoring in large-animal models (dogs), using 75 mg/kg dose IV administration (5x MTD for IV route). Using the body surface area (BSA) scaling factor canine equivalent dose (CED) (mg/kg) = Mouse dose (mg/kg) * (Mouse Km/Canine Km)) where Km is the BSA scaling factor, to estimate the canine equivalent dose from mouse studies.[27] This dose factor for safety-toxicity and PK analysis was 0.15.[27] We assessed the impact of extremely high doses (e.g. 5x MTD using IV administration) or potential acute drug toxicity in a large-animal model (dogs). We monitored these animals over the recommended 14-day period, with extensive clinical sign monitoring and health checkups (**Fig. S3**), and detailed biomarker assessment, as shown in **Fig.1C-F**. We dosed dogs using IV and SQ at 75 mg/kg dose. While few test subjects showed some short-term AEs noted in **Fig. S3**, and 75 mg/kg dose was marked as above MTD in our studies, we sought to further evaluate any adverse health impact. Using a battery of complete blood count (CBC)/chemistry tests for potential immunogenic response (by monitoring neutrophils, lymphocytes, monocytes, or eosinophils in blood, **Fig. 1C**), overall health (total protein TP, albumin A, globulin G, and A/G ratio, **Fig. 1D**), liver enzymes (T-bilirubin, alkaline phosphatase (ALP), alanine transaminase (ALT), gamma-glutamyl transferase (GGT), **Fig. 1E**), and metabolic markers (like cholesterol, creatine kinase, glucose, and plasma protein, **Fig. 1F**), we did not observe any pathogenic change in any test subject. We also monitored red blood cells, electrolytes (**Fig. S4**), and kidney function (**Fig. S5**) for the acute-dosed beagle dogs to assess any adverse health impact through these biochemical markers. We did not observe any lasting health effects throughout the biomarker assays and the 14-day clinical monitoring. We also repeated these studies at the estimated MTD values for different routes (**Figs. S6-S9**), but again did not observe any abnormal values or clinical concern in any test subject. This showed a well-tolerated, non-toxic, and non-pathogenic safety profile of API Nanoligomer NI112 treatment using extremely high (acute) dosing in large-animals.

Modeling Biodistribution of the API in Blood Serum and Target Organs

We measured API NI112 concentration (using ICP-MS, see Methods) in blood for 4-different administration routes (IV, IP, IN, and SQ) in mice, with time, and used the multiexponential decay to estimate the time-dependent bound and unbound API concentration (**Fig. 2A**). Briefly, the longtime-decay exponential of blood serum API (bound serum) was assessed as a fraction of the unbound API (**Fig. 2B-E**), and observed the unbound API decays with time, almost completely disappearing within 24-hours of drug administration in mice. Another important observation was that while IV and IP routes exhibited an appreciable unbound/bound API ratio (**Fig. 2B, D**), SQ and IN routes had a very low ratio of unbound API measured in blood (**Fig. 2C, E**). Eventually (~24 hours post-administration) all the measured API is bound. These results are consistent with our prior studies, which tracked any unbound API (and all missense sequences) cleared through urine by the animals.[19,20] We also used PK solver[28] to derive pharmacokinetic

parameters for the API in blood serum and measurement of biodistribution coefficient ($F=AUC_{Test\ route}/AUC_{I.V.}$, AUC: Area under the curve), as shown in **Figs. S10, S11**. While IV and SQ routes showed rapid uptake in the blood (T_{max} 2 hours) compared to IP and IN, the target organ brain tissue concentration showed higher variance. The half-life in blood (~1-2 days) was also significantly lower than in the brain (~ 1-2 weeks), showing the rapid uptake of API in different organs and drug clearance from the bloodstream through urine.[19,20]

Further measurements of API NI112 were done in the target organ (the brain, **Figs. 3, 4**) and other potential target and/or first pass, and clearance organs (liver, kidney, colon, **Fig. 5**). We found high drug bioavailability (~30% of the drug) in the brain across the BBB, compared to API concentration in the blood, and much higher values in liver, kidney, and colon. We even observed excellent biodistribution among different brain regions (hippocampus, thalamus, cortex, cerebellum, and brainstem, **Fig. 3C**), providing good confidence for drug delivery and using other Nanoligomer target sequences for different neuronal disease applications. We also developed a model for predicting target organ concentration and precise dosing concentration and dose frequency (**Fig. 4**). The predictive nature of such PK/PD biodistribution profile, combined with detailed disease model studies in small-animals could provide an excellent platform using dose scaling and similar interspecies translation parameters for large-animal model.

Biodistribution in the Large-Animal Model (Dogs):

We measured NI112 concentration with time in blood serum for IV, and SQ dosing in dogs (**Figs. 6-8**). We obtained PK parameters for different routes and concentrations used (**Figs. S10, S12**). The PK parameters showed similar peak API concentration as rodents, but significantly higher bound API concentrations with time, and much higher AUC values, due to higher target mRNA and protein concentration (NF-κB and NLRP3) in dogs than mice, well beyond BSA scaling used. These AUC ratios also correspond with interspecies scaling and are better predictors than BSA estimation (Km ratios) used for dose scaling between mice and dog studies. We also modeled multiexponential decay to estimate the bound and unbound API concentration with different IV (**Fig. 6**) and SQ (**Fig. 7**) doses. Our model showed a strong predictive, linear relationship (ratios/slope slightly lower than 1) between the bound serum API concentration with time and dose ratios (**Fig. 8**). Therefore, our PK parameters and the model showed an excellent biodistribution profile for the API NI112, and very predictive dose scaling for both small- and large-animal models. Therefore, we proceeded to combine our model results (small- and large-animal) to develop interspecies scaling and translation parameters for the API NI112.

Translation and Scaling across Species (Between Small- and Large-Animal Models)

Using the detailed PK, biodistribution, and scaling models for large- and small-animals, we attempted to develop interspecies scaling and translation parameters. While the proposed BSA scaling utilized the Km ratio as a simplistic model,[27] several studies have highlighted the inadequateness of such simple model scaling and the need for more concrete (area under the curve AUC) and other PK and biodistribution-based modeling parameters to scale.[29] We observed that even though the doses were BSA-scaled between large-animal (dog) and small-animal (mice) studies for both IV and SQ administration of API based on Km (Km dose factor for dog/mice was 0.15), the value we observed for two routes was not one (**Fig. 9**). Using the

ratio of these scaled doses between species, we observed a clear ratio of 5-6.5 for SQ, and between 12-15 for IV administration, presumably based on accessible target ratio (NF-κB and NLRP3 protein amount between species) and AUC ratios (**Fig. 9**). Our previous studies showed that 150 mg/kg NI112 IP dosing in mice was therapeutic in several neurological diseases.[17,22,23] Based on dose scaling for different routes in mice shown here (**Fig. 4**), it corresponds to 50 mg/kg SQ and 30 mg/kg IV dosing in mice. For interspecies scaling, using both BSA (factor 0.15) and SQ and IV factors shown in Fig. 9, CED corresponds to 1.5 mg/kg SQ and 0.35 mg/kg IV dosing in dogs, and using BSA scaling from dog to human, an estimated human equivalent dose (HED) of 0.5-0.75 mg/kg SQ and 0.175 mg/kg IV. For a 70 kg human, this roughly translates to therapeutic dosing of 35-52 mg API through SQ and 12.5 mg dosing through IV. We continue to develop a predictive model for further scaling for human translation but can use these models and scaling/translation ratios to provide a better estimate for HED. Together, the developed model and pharmacological biodistribution parameters obtained provide a good foundation for further translation and assessment of the API.

CONCLUSIONS:

In conclusion, we conducted a detailed safety-toxicity assessment (long-term repeat dosing and extremely high 5x MTD acute dosing) in small- (C57BL/6 mice) and large-animal (beagle dogs) models for assessment of neurotherapeutic API NI112. We assessed histological, detailed biochemical (through multiplexed ELISA), and extensive CBC/chemistry biomarker monitoring of immune, metabolic, liver, kidney, and cardiac function. Not a single test subject showed any lasting health impact of the drug administration, and no evidence of any immunogenic response, drug accumulation, tissue damage, or immune cell infiltration was observed. Overall, the animals showed that the new Nanoligomer modality has a strong safety profile. We also conducted detailed PK and biodistribution studies using different routes of administration (IV, SQ, IP, IN) at different doses, and obtained relevant PK parameters. We observed high biodistribution across the target organ the brain (~30% of API in the brain across BBB, compared to that bound in blood serum), and across the different brain regions (the hippocampus, thalamus, cortex, cerebellum, and the brain stem) and high therapeutic bioavailability (>15-40 K_D) for low/moderate dosing, and effective target engagement. We found good agreement between administered dose ratios and measured API across the blood serum, the brain, and other first-pass and clearance organs, as well as good agreement between interspecies parameters obtained. While the simple BSA scaling did not provide directly translatable doses (BSA-scaled doses across species do not result in ratios of 1), the values obtained here can provide an excellent starting point/platform for further testing and clinical translation of the API for inflammatory and CNS diseases.

METHODS:

Nanoligomer Synthesis

NFκB and NLRP3 antisense Nanoligomers were synthesized at Sachi Bio following established methods detailed elsewhere.[17–22] Briefly, 17-base-long peptide nucleic acid (PNA)[17,18,21,30] sequence was selected to optimize solubility and specificity, targeting the start codon regions of *nfkb1* (Sequence: AGTGGTACCGTCTGCTA) and *nlrp3* (Sequence: CTTCTACTGCTCACAGG), within the Mouse genome (GCF_000001635.27), identified using our bioinformatics toolbox.[21] The PNA was synthesized on a Vantage peptide synthesizer (AAPPTec, LLC) using solid-phase Fmoc chemistry. Fmoc-PNA monomers, wherein A, C, and G monomers were shielded with Bhoc groups, were obtained from PolyOrg Inc. Post-synthesis, the peptides were attached to gold nanoparticles and subsequently purified using size-exclusion filtration. The conjugation process and the concentration of the purified Nanoligomer was measured using absorbance at 260 nm (for PNA detection) and 400 nm (for nanoparticle quantification).

In vivo mice studies

Adult female and male C57Bl6/J mice purchased from Jackson Laboratories were housed throughout all experiments at ~18-23°C on a 12-light/12-dark cycle. Fresh water and *ad-libitum* food (Tekland 2918; 18% protein) was routinely provided to all cages. Animals were consistently health checked by the veterinary staff at Colorado State University (CSU). This protocol was approved by the CSU Institutional Animal Care and Use Committee (IACUC) and Laboratory Animal Resources staff.

Tissue collection

Mice were culled after deep anesthetizing with isoflurane, and ~1 ml of blood was removed via cardiac puncture followed by cervical dislocation. The brain was sliced sagittally and the right side of the brain was fixed in 10% normal buffered formalin (NBF) and the left hippocampus, thalamus, brainstem, and a piece of the left cortex and cerebellum tissue were removed, flash-frozen, and stored at -80°C until further processing. The liver, kidney, and colon were also removed, fixed in 10% NBF, and processed (paraffin-embedded) for immunostaining (details below).

Large-animal dog studies

All aspects of the study were approved by the CSU IACUC (protocol ID 4320, approved April 18, 2023). Fifteen healthy, purpose-bred, mixed-sex (14 female, 1 male) beagles between 2 and 3 years of age were enrolled. Dogs weighed a mean of 8kg with a range of 6.7 to 10.6kg. All animals were housed in an on-site research facility and were fed, cleaned, socialized, and examined daily by Laboratory Animal Resource staff or veterinarians. Due to animal temperament and intergroup aggression, dogs were housed in 1 group of 5 dogs, 2 groups of 3 dogs, and 2 groups of 2 dogs. Each dog was identified by a distinct ear tattoo. Dogs were offered water continuously and were fed Exclusive Adult Dog Chicken & Brown Rice Formula dry food

in the mornings. Blood samples were collected at time t=0, 2, 4, 8, 12, 24, 48 hours, 7, and 14 days.

VCOG Grading scale	
1	Mild; asymptomatic or mild symptoms, clinical signs, or diagnostic observations only; interventions not indicated
2	Moderate; outpatient or non-invasive intervention indicated; moderate limitation of Activities of Daily Living (ADL)
3	Severe or medically significant but not immediately life-threatening; hospitalization or prolonged hospitalization indicated; disabling, significantly limiting ADL
4	Life-threatening consequences; urgent interventions indicated
5	Death related to AE

Multiplexed ELISAs

Blood serum and tissue homogenates from mice were subjected to analysis using the ThermoFisher 36-plex Procartaplex cytokine/chemokine panel. [17,18] The process involved homogenizing 25uL of 10 mg/ml brain tissues with ProcartaPlex™ Cell Lysis Buffer (ThermoFisher) and 5-mm stainless steel beads (Qiagen) at 25 Hz for 1.5-3 minutes, utilizing a Qiagen/Retsch Bead Beater. After homogenization, samples underwent centrifugation at 16,000 x g for 10 minutes at 4 °C. Following centrifugation, homogenized samples were evaluated for protein concentration using the DC Protein Assay (Bio-Rad) kit protocol. Protein measurements were acquired through a Tecan GENios microplate reader.

The homogenate was then processed in accordance with the manufacturer's provided protocol and analyzed using a Luminex MAGPIX xMAP instrument. Standards for each cytokine/chemokine were utilized at 1:4 dilutions (8-fold dilutions), alongside background and controls. Subsequently, sample concentrations were determined from a standard curve using the Five Parameter Logistic (5PL) curve fit/quantification method.

Inductively coupled plasma mass spectrometry (ICP-MS)

ICP-MS quantification was conducted following established protocols as outlined in prior publications.[19,20] Briefly, tissue samples underwent homogenization in a TissueLyser II bead mill (Qiagen, Germantown, MD) at 30 Hz for 3 minutes, with the addition of 1 µl deionized water per 1 mg of organ tissue. Homogenates were subsequently digested in 500 µl of aqua regia (3:1 hydrochloric acid to nitric acid) for 4 hours at 100 °C. Pellets resulting from the digestion process were resuspended in water and subjected to analysis using a NexION 2000B single quadrupole ICP-MS system (PerkinElmer, Waltham, MA). The sample introduction utilized a Meinhard nebulizer with a cyclonic glass spray chamber, and a nickel sample and skimmer cone were employed in conjunction with an aluminum hyperskimmer cone. A seven-point linear standard curve was generated within a concentration range of 0-250 ppb Au, and linearity was defined at an R^2 value of greater than 0.995. The 1000 ppm gold standard solution (Ricca

Chemical Company, Arlington, TX), and TraceMetal grade 70% HNO_3 (ThermoFisher Scientific, Waltham, MA) were used as obtained. All water used was sourced from a Milli-Q system (Millipore, Burlington, MA). Subsequent data analysis was carried out using Microsoft Excel.

Hematoxylin and Eosin staining for tissue morphology

Brains and visceral organs were fixed in 10% NBF at room temperature for at least 48 hours. Tissues were processed using a Leica TP1020 Automatic Benchtop Tissue Processor and embedded in paraffin wax (Cancer Diagnostics, Cat #: EEPAR56). Tissues were sectioned on a ThermoFisher Scientific HM 325-2 Manual Microtome at 5μm thickness and mounted on positively charged glass slides (Superfrost Plus, Cancer 232 Diagnostics, Cat #: 4951) for staining and analysis. One section per animal was deparaffinized and stained with hematoxylin (Cancer Diagnostics, Cat#: #HTV-4) and eosin (Cancer Diagnostics, Cat#: #ETV) (H&E) for the determination of histopathological changes. Whole tissue images were taken for analysis using an Olympus DP70 camera using an Olympus UPlanSApo 20x objective (N.A. = 0.75).

Statistics

Statistical tests, numbers of mice, and p-values are indicated in figure legends. GraphPad Prism and Microsoft Excel were used for statistical analysis.

Ethics Approval

Mice were euthanized by deeply anesthetizing with isoflurane followed by decapitation. All mice were bred and maintained at Lab Animal Resources, accredited by the Association for Assessment and Accreditation of Lab Animal Care International, in accordance with protocols approved by the Institutional Animal Care and Use Committee at Colorado State University. All dog experimentation was also approved by the Clinical Review Board and the Institutional Animal Care and Use Committee at Colorado State University.

Funding

Authors acknowledge financial support from NASA SBIR Award 80NSSC22CA116.

Author Contributions

P.N. conceived the idea, designed the experiments, and synthesized the Nanoligomers. J.A.M. and S.M. designed and supervised animal studies. S.R. and J.A.M. conducted the small-animal mice studies, tissue dissections, immunofluorescence, and scoring. S.S. and V.G. homogenized the tissues, carried out sample digestions and sample preparation for ICP-MS, and conducted ELISA (with P.N.). B.K., M.A., and S.M. conducted all dog studies and sample collections. S.B. and J.B. conducted ICP-MS measurements. P.N. and A.C. wrote the manuscript with input from all the authors. All authors read the manuscript and provided input.

Notes

Declaration of competing interests

S.S., V.G., A.C., and P.N. work at Sachi Bio, a for-profit company, where the Nanoligomer technology was developed. A.C. and P.N. are the founders of Sachi Bio, and P.N. has filed a patent on this technology. Other authors declare no competing interest.

FIGURES:

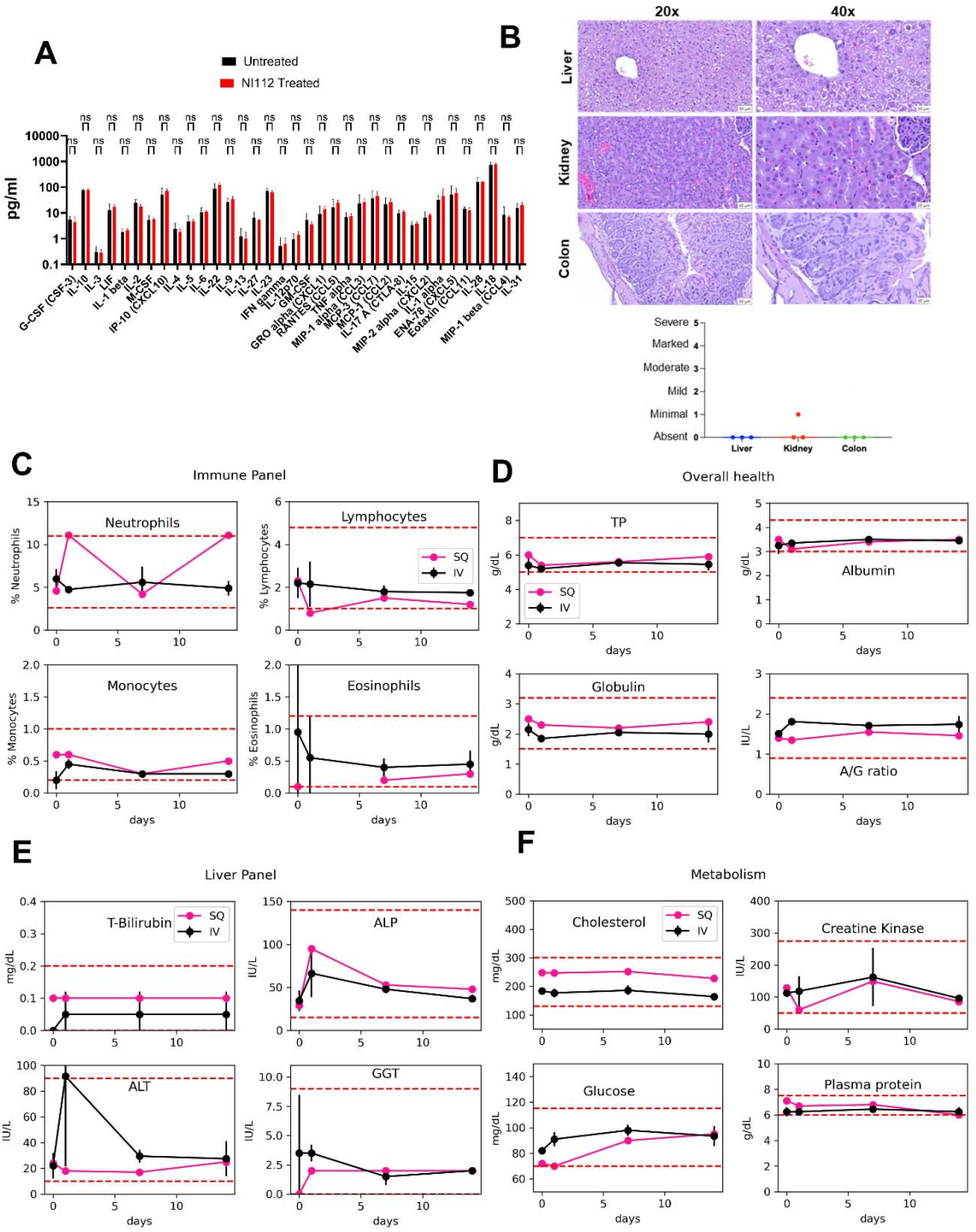

Fig.1. Long-term safety-toxicity and acute single-dose studies reveal the high safety profile of NI112 Nanoligomer. A) 12-week dosing of NI112 3x a week shows no change in the immune profile of mice blood serum, as shown using 36-plex cytokine and chemokine markers, measured for treated and untreated animals (n=4/group), ns = non-significant using unpaired t-test for each

cytokine. **B)** H&E-stained histology of kidney, liver, and colon samples from mice after high-dose (150 mg/kg 3x a week) long-term (12-weeks) treatment shows no immune cell infiltration or any immunogenic response. Histologic findings in each tissue were diagnosed and graded for severity on a 0-5 scale based on inflammation and hemorrhage; 0=absent, 1=minimal (10% of tissue affected), 2=mild (10-25% of tissue affected), 3=moderate (26-50% of tissue affected), 4=marked (51-75% of tissue affected), 5=severe (75% of tissue affected). There were no significant histologic findings/differences in the liver, kidney, or colons of mice treated with NI112. Kidney nephrons displayed no evidence of inflammation within the glomeruli, supporting the renal clearance shown previously for Nanoligomer molecules.[19,20] **C)** Immune panel studies of dogs treated with 75 mg/kg NI112 Dog which corresponds to 500 mg/kg dosing in mice, and is well above the MTD. Dogs were monitored for 2 weeks post-administration. The results show a lack of any immunogenic response, and no change in neutrophils, lymphocytes, monocytes, or eosinophils in blood. **D)** Similar assessment of overall health using total protein (TP), albumin (A), globulin (G), and A/G ratio. **E)** Assessment of the liver panel of these animals, and **F)** Metabolism. The red dashed lines show upper and lower normal limits for each measurement. The curves show mean values and bars show standard deviation (Mean ± Standard Deviation, SD). These extensive studies show minimal side effects and a lack of long-term health concerns even at such high acute doses.

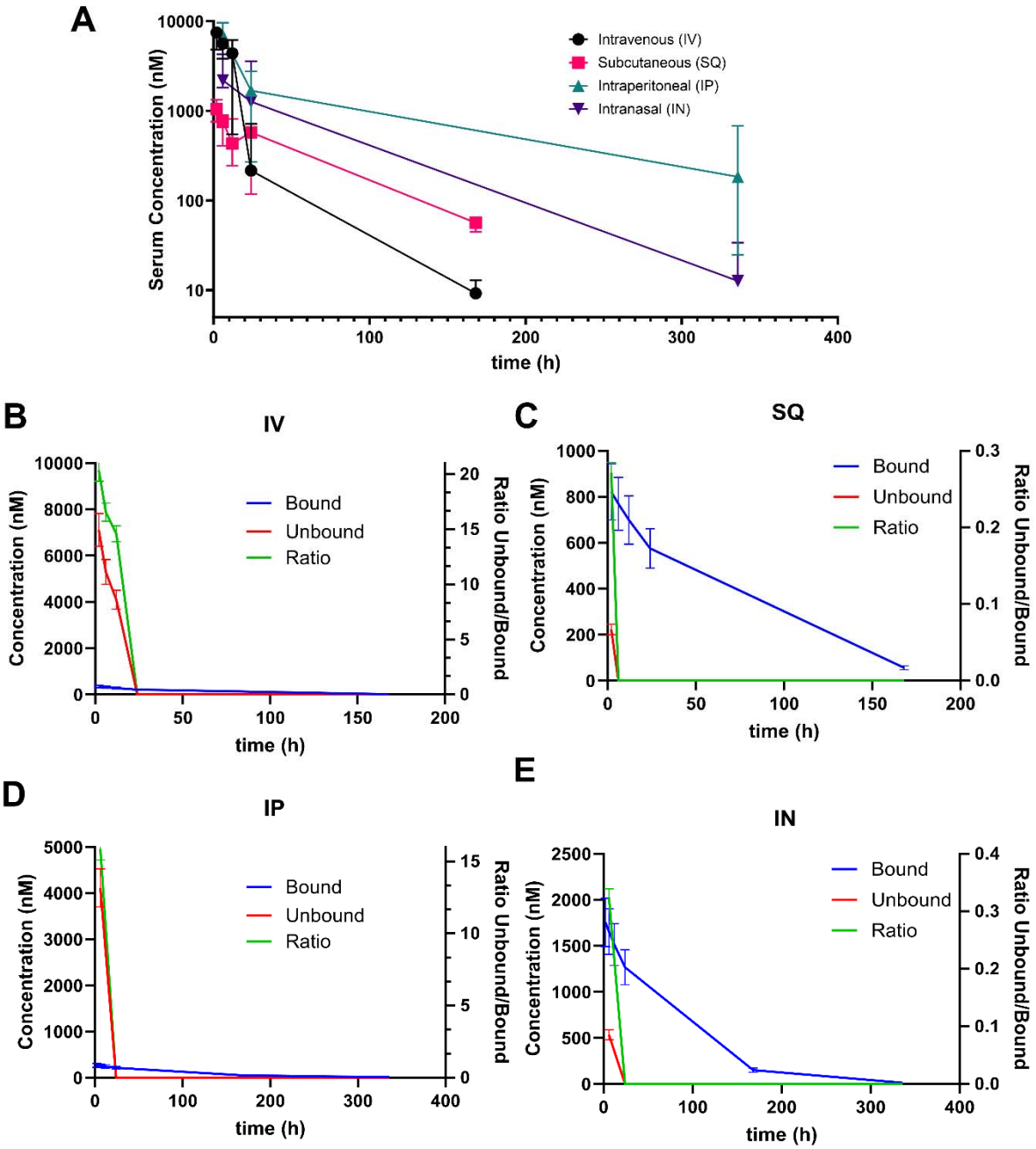

Fig.2. Bound and Unbound API NI112 with time using different routes of administration. A) Mice studies showing NI112 concentration in blood serum with time using 4 different routes of administration at MTD IV (100 mg/kg), IP (500 mg/kg), SQ (450 mg/kg), and IN (500 mg/kg). The multiexponential decay with time was used to derive bound and unbound API (NI112) concentration with time using **B)** IV; **C)** SQ; **D)** IP; and **E)** IN route. Right Y axis shows the ratio of unbound/bound API in blood serum. The curves show Median values, with the bars

showing variance (Median ± SE). Number of animals n=4/group for IV and SQ, n=6/group for IN and IP route of administration.

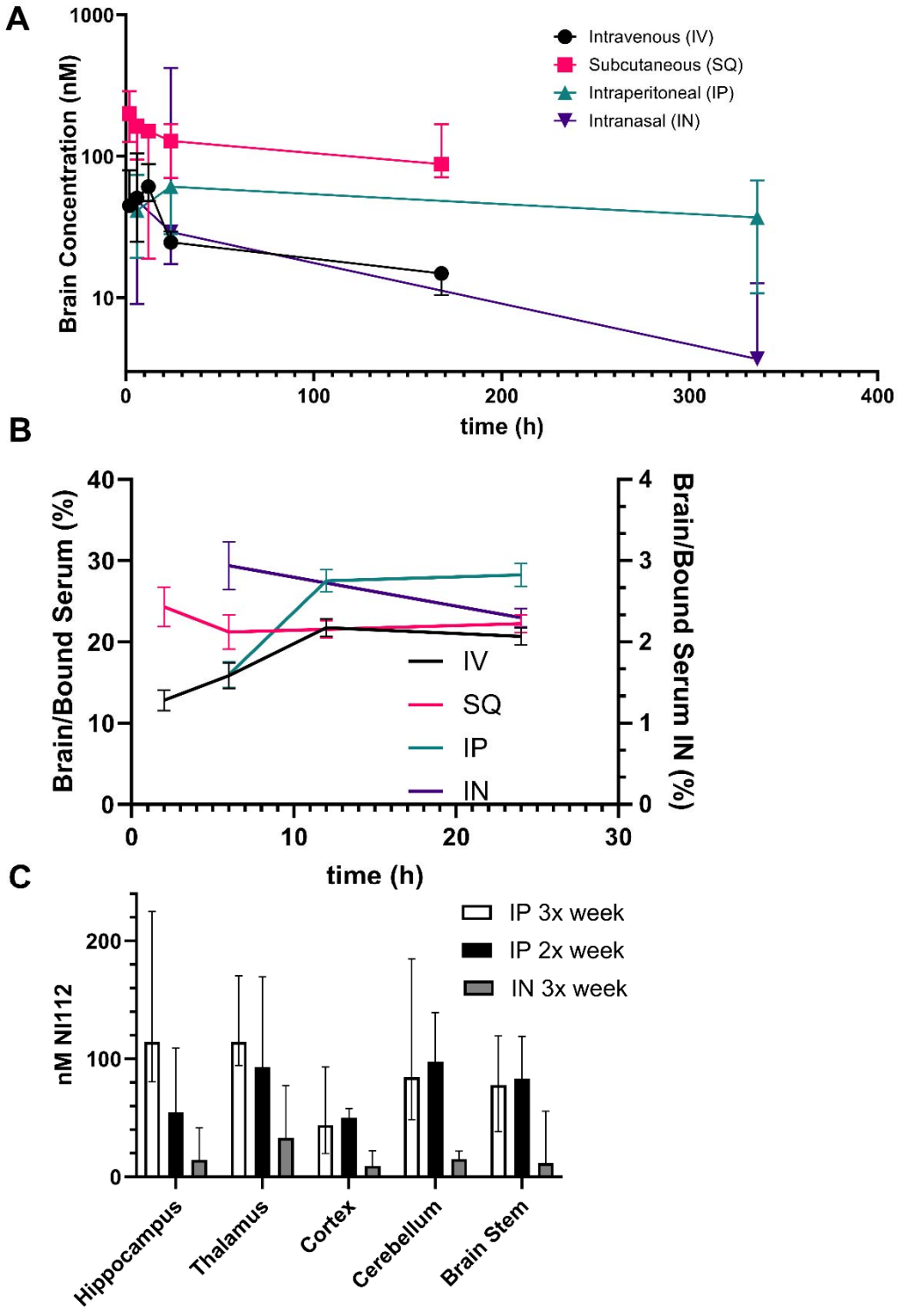

Fig. 3. High drug bioavailability and BBB-crossover for neurological disease application. A) Mice studies showing NI112 concentration in brain tissue with time using 4 different routes of administration at MTD IV (100 mg/kg), IP (500 mg/kg), SQ (450 mg/kg), and IN (500

mg/kg). **B)** Ratio of Brain tissue to bound API concentration in blood serum shows a fairly consistent value (~25-30%) for 3 routes of administration IV, IP, and SQ. Right Y axis shows the ratio of brain tissue/bound API in blood serum for IN administration which is one order of magnitude lower (~3%). **C)** High bioavailability of API (NI112) in different brain regions with different dosing regimens (3x a week and 2x a week) using IP and IN route at 150 mg/kg dose. The curves show Median values, with the bars showing variance (Median ± SE). Number of animals n=4/group for IV and SQ, n=6/group for IN and IP route of administration.

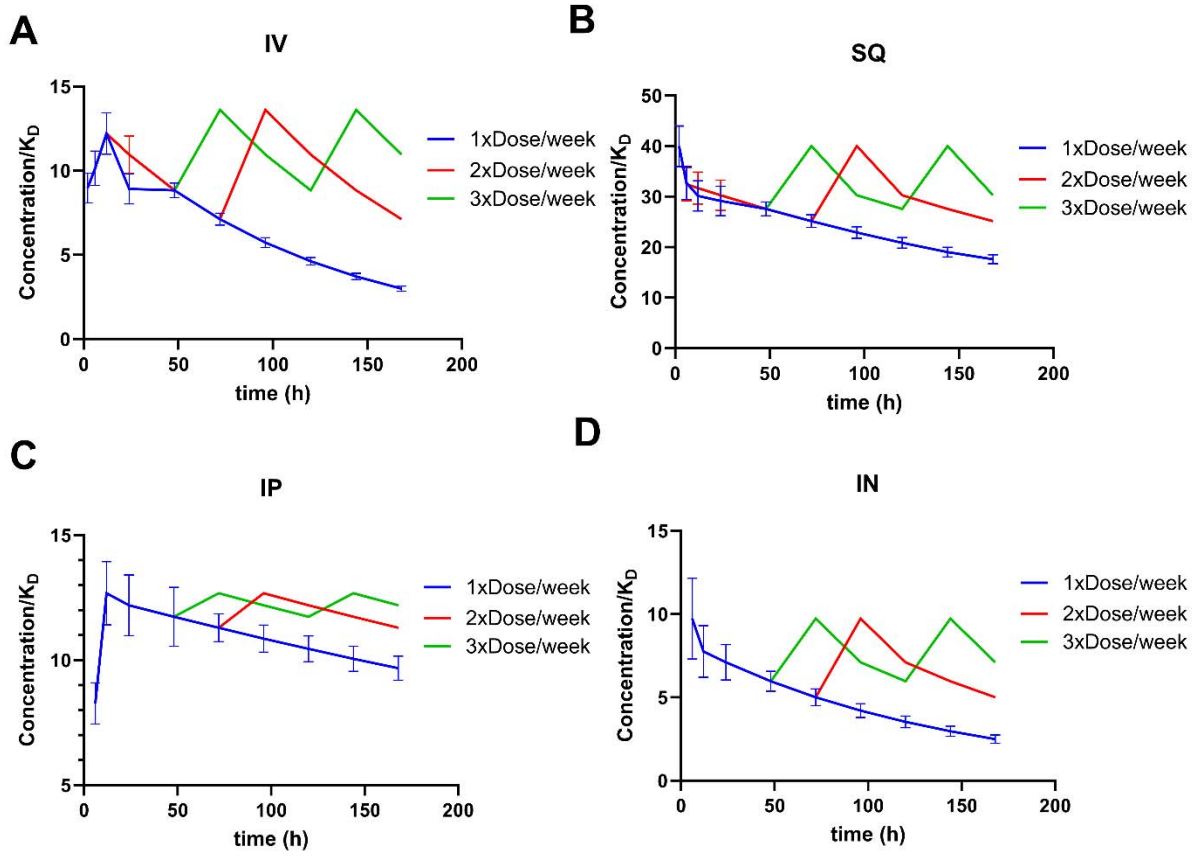

Fig. 4. Dosing and repeat dose modeling data for small-animal studies in the target organ (the brain). A) IP administration of API NI112 concentration in brain tissue normalized with drug K_D (5 nM, Nanoligomer measured K_D of 3.37 nM,[19,20] other PNA studies show values 5-8 nM[25]) with time using IV (100 mg/kg dosing). The blue curve with standard deviation shows the measured values after a single dose at MTD, whereas red (2x a week) and green (3x a week) are modeled values, shown without SE for clarity. **B)** SQ dosing (450 mg/kg) showing single and repeat dosing effects on target organ (the brain) concentration normalized by K_D. **C)** IP (500 mg/kg) and **D)** IN (500 mg/kg) show high drug bioavailability of API (NI112) in brain regions with different dosing regimens (3x a week and 2x a week). The curves show Median values, with the bars showing variance (Median ± SE). Number of animals n=4/group for IV and SQ, n=6/group for IN and IP route of administration.

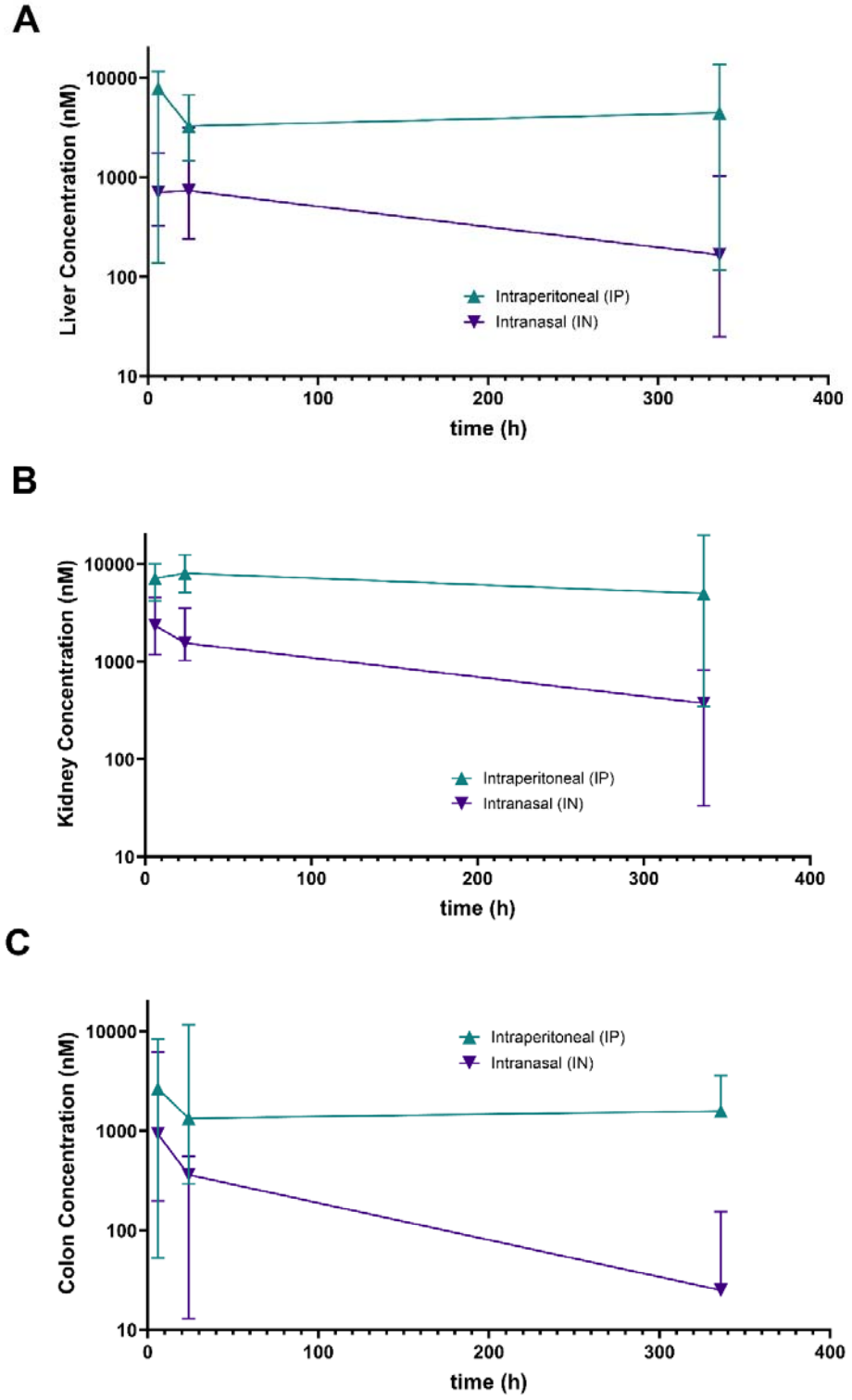

Fig. 5. NI112 tissue concentration in the first pass and clearance organs. Mice studies showing NI112 concentration in different first pass and clearance organ tissues with time using IP and IN routes of administration **A)** Liver, **B)** Kidney, and **C)** Colon. The curves show Median

values, with the bars showing variance (Median ± SE). Number of animals n=6/group for IN and IP route of administration.

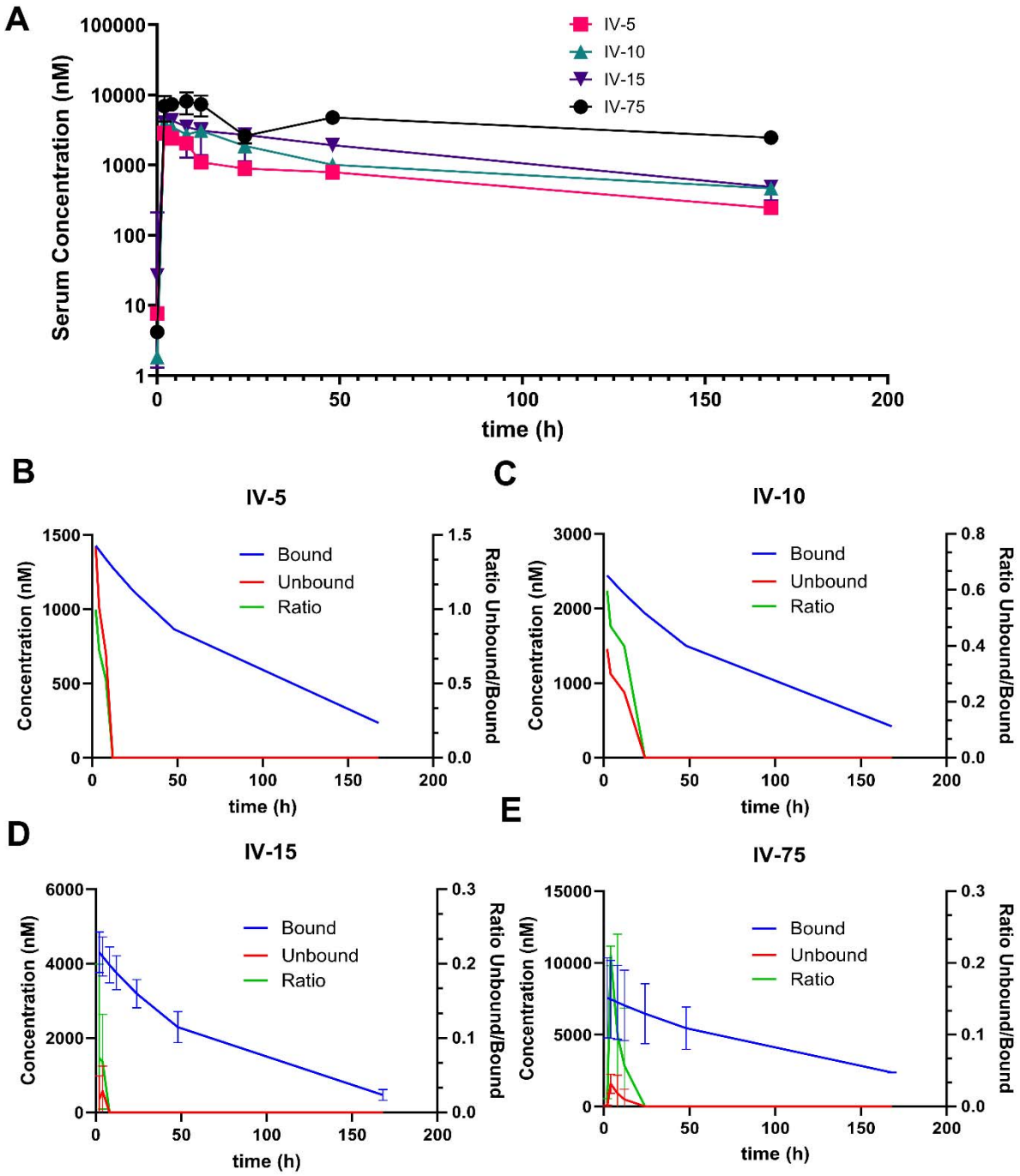

Fig. 6. Large-animal dog studies using IV administration of API NI112 at different concentrations. A) Blood serum concentration of the API with 5, 10, 15, and 75 mg/kg dosing in beagle dogs. Multiexponential decay of API concentration was used to determine bound and unbound serum concentrations for: **B)** 5 mg/kg; **C)** 10 mg/kg; **D)** 15 mg/kg (MTD, n=3/group); and **E)** 75 mg/kg (5xMTD) IV dose. The blue curve (bound) and red curve (unbound) show API

in blood, along with the Ratio of unbound/bound API (green curve, shown on Right Y-axis). The curves show Median values, with the bars showing variance (Median ± SE).

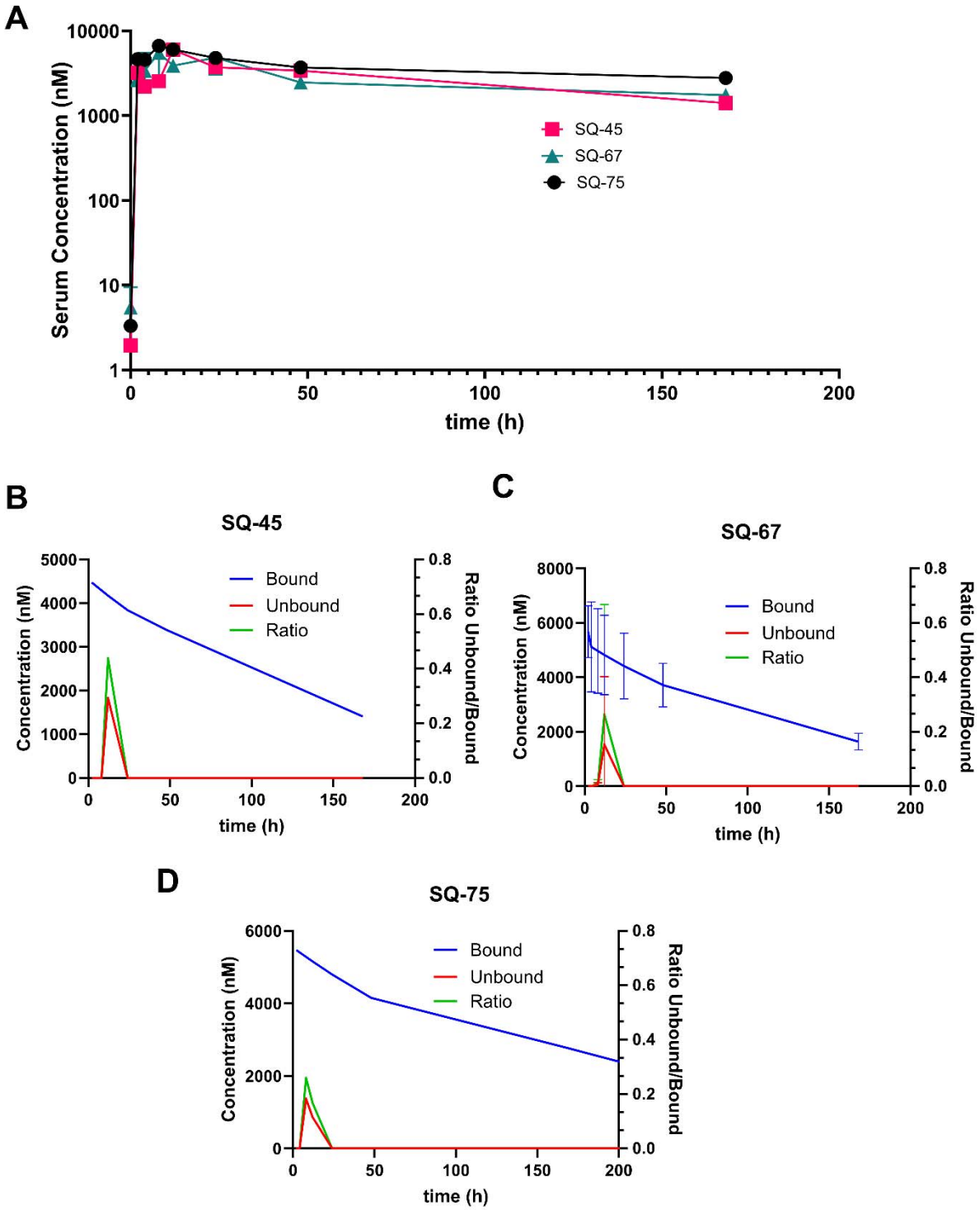

Fig.7. Large-animal dog studies using SQ administration of API NI112 at different concentrations. A) Blood serum concentration of the API with 45, 67, and 75 mg/kg dosing in beagle dogs. Multiexponential decay of API concentration was used to determine bound and

unbound serum concentrations for: **B)** 45 mg/kg; **C)** 67 mg/kg; **D)** 75 mg/kg SQ dose. The blue curve (bound) and red curve (unbound) show API in blood, along with the Ratio of unbound/bound API (green curve, shown on Right Y-axis). The curves show Median values, with the bars showing variance (Median ± SE).

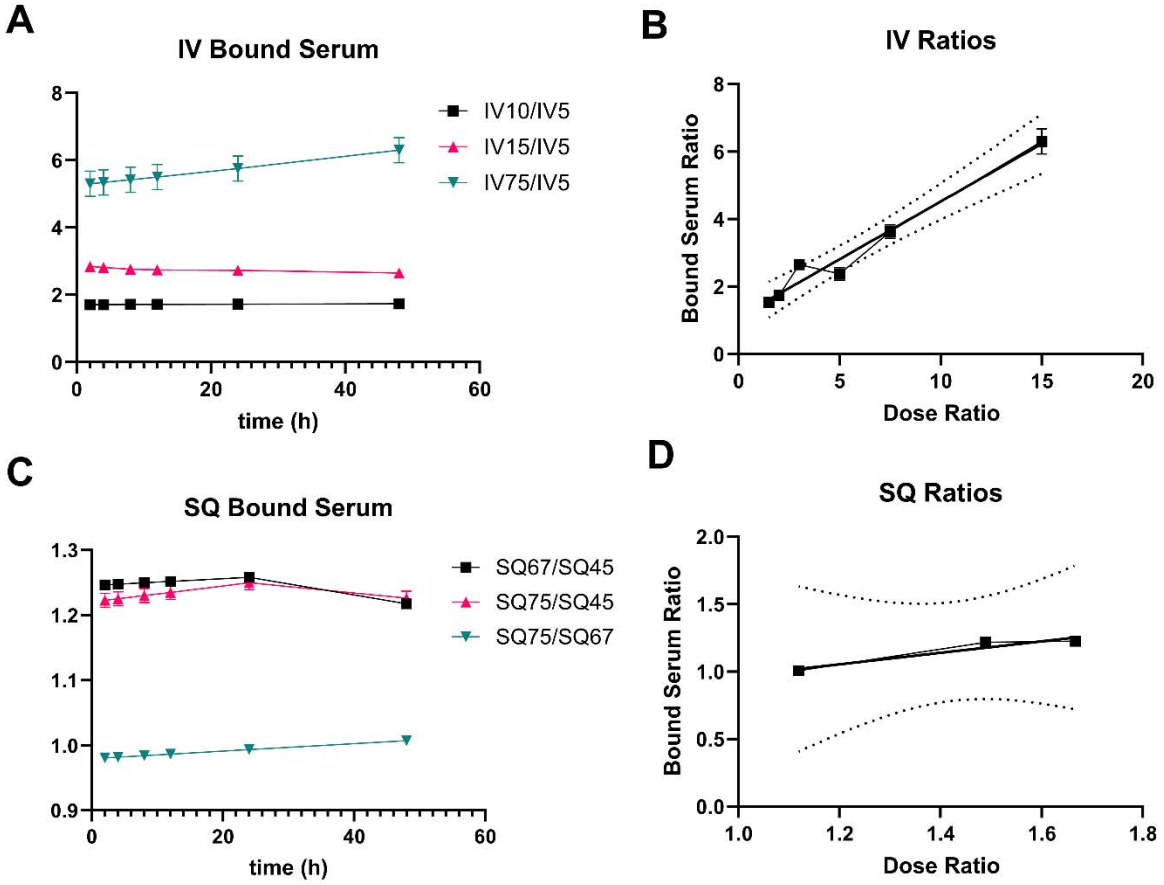

Fig.8. Dose scaling in dog studies using IV and SQ administration of API NI112 at different concentrations. A) IV concentration of bound serum shows a nearly constant ratio with the lowest concentration (5 mg/kg). The ratio of 75/5 mg/kg (inverted triangle), 15/5 mg/kg (upward triangle), and 10/5 mg/kg (square) shows flatline values. **B)** Linear regression between the bound serum ratio and the dose ratio, with dashed curves showing the 5% and 95% confidence intervals. **C)** Bound serum ratio between respective SQ doses. **D)** Linear regression between bound serum ratio and dose ratio, showing easily predictable dose scaling that can be used to determine dosing and target organ concentrations in large-animals (beagle dogs). The curves show bound API from Median values, and the bars show variance.

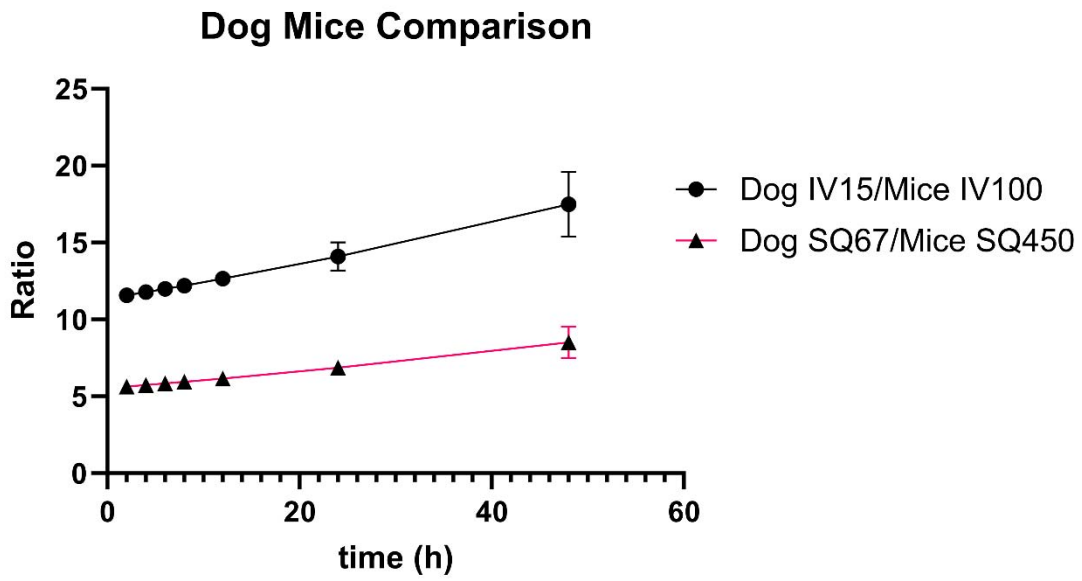

Fig.9. Scaling between large-animal (dog) and small-animal (mice) studies using IV and SQ administration of API NI112 at different concentrations. The doses chosen were based on the Km scaling described above (CED (mg/kg) = Mouse dose (mg/kg) * (Mouse Km/Canine Km)) to estimate the canine equivalent dose from mouse studies. The dose factor for dogs/mice was 0.15.[27] The curves show ratios estimated from Median values, with the bars showing variance.

References:

(1) US Department of Health and Human Services. Progress in Autoimmune Diseases Research. *Natl. Institutes Heal.* **2005**, *05–5140* (5).

(2) Cooper, G. S.; Bynum, M. L. K.; Somers, E. C. Recent Insights in the Epidemiology of Autoimmune Diseases: Improved Prevalence Estimates and Understanding of Clustering of Diseases. *J. Autoimmun.* **2009**, *33* (3–4). https://doi.org/10.1016/j.jaut.2009.09.008.

(3) Fairweather, D. L.; Rose, N. R. Women and Autoimmune Diseases. In *Emerging Infectious Diseases*; 2004; Vol. 10. https://doi.org/10.3201/eid1011.040367.

(4) Heneka, M. T. Inflammasome Activation and Innate Immunity in Alzheimer's Disease. *Brain Pathol.* **2017**, *27* (2). https://doi.org/10.1111/bpa.12483.

(5) Ising, C.; Venegas, C.; Zhang, S.; Scheiblich, H.; Schmidt, S. V.; Vieira-Saecker, A.; Schwartz, S.; Albasset, S.; McManus, R. M.; Tejera, D.; Griep, A.; Santarelli, F.; Brosseron, F.; Opitz, S.; Stunden, J.; Merten, M.; Kayed, R.; Golenbock, D. T.; Blum, D.; Latz, E.; Buée, L.; Heneka, M. T. NLRP3 Inflammasome Activation Drives Tau Pathology. *Nature* **2019**, *575* (7784). https://doi.org/10.1038/s41586-019-1769-z.

(6) Ní Chasaide, C.; Lynch, M. A. The Role of the Immune System in Driving Neuroinflammation. *Brain Neurosci. Adv.* **2020**, *4*. https://doi.org/10.1177/2398212819901082.

(7) Wes, P. D.; Easton, A.; Corradi, J.; Barten, D. M.; Devidze, N.; DeCarr, L. B.; Truong, A.; He, A.; Barrezueta, N. X.; Polson, C.; Bourin, C.; Flynn, M. E.; Keenan, S.; Lidge, R.; Meredith, J.; Natale, J.; Sankaranarayanan, S.; Cadelina, G. W.; Albright, C. F.; Cacace, A. M. Tau Overexpression Impacts a Neuroinflammation Gene Expression Network Perturbed in Alzheimer's Disease. *PLoS One* **2014**, *9* (8). https://doi.org/10.1371/journal.pone.0106050.

(8) Yasir, M.; Goyal, A.; Sonthalia, S. Corticosteroid Adverse Effects. In *StatPearls*; 2022.

(9) Jung, S. M.; Kim, W. U. Targeted Immunotherapy for Autoimmune Disease. *Immune Network*. 2022. https://doi.org/10.4110/in.2022.22.e9.

(10) Villoslada, P.; Moreno, B.; Melero, I.; Pablos, J. L.; Martino, G.; Uccelli, A.; Montalban, X.; Avila, J.; Rivest, S.; Acarin, L.; Appel, S.; Khoury, S. J.; McGeer, P.; Ferrer, I.; Delgado, M.; Obeso, J.; Schwartz, M. Immunotherapy for Neurological Diseases. *Clinical Immunology*. 2008. https://doi.org/10.1016/j.clim.2008.04.003.

(11) Chimalakonda, A.; Burke, J.; Cheng, L.; Catlett, I.; Tagen, M.; Zhao, Q.; Patel, A.; Shen, J.; Girgis, I. G.; Banerjee, S.; Throup, J. Selectivity Profile of the Tyrosine Kinase 2 Inhibitor Deucravacitinib Compared with Janus Kinase 1/2/3 Inhibitors. *Dermatol. Ther. (Heidelb).* **2021**, *11* (5). https://doi.org/10.1007/s13555-021-00596-8.

(12) Rinaldi, C.; Wood, M. J. A. Antisense Oligonucleotides: The next Frontier for Treatment of Neurological Disorders. *Nature Reviews Neurology*. 2018. https://doi.org/10.1038/nrneurol.2017.148.

(13) Mazur, C.; Powers, B.; Zasadny, K.; Sullivan, J. M.; Dimant, H.; Kamme, F.; Hesterman, J.; Matson, J.; Oestergaard, M.; Seaman, M.; Holt, R. W.; Qutaish, M.; Polyak, I.; Coelho, R.; Gottumukkala, V.; Gaut, C. M.; Berridge, M.; Albargothy, N. J.; Kelly, L.; Carare, R. O.; Hoppin, J.; Kordasiewicz, H.; Swayze, E. E.; Verma, A. Brain Pharmacology of Intrathecal Antisense Oligonucleotides Revealed through Multimodal Imaging. *JCI Insight* **2019**, *4* (20). https://doi.org/10.1172/jci.insight.129240.

(14) Goto, A.; Yamamoto, S.; Iwasaki, S. Biodistribution and Delivery of Oligonucleotide Therapeutics to the Central Nervous System: Advances, Challenges, and Future Perspectives. *Biopharmaceutics and Drug Disposition*. 2023. https://doi.org/10.1002/bdd.2338.

(15) Geary, R. S.; Yu, R. Z.; Siwkowski, A.; Levin, A. A. Pharmacokinetic/Pharmacodynamic Properties of Phosphorothioate 2′-O-(2-Methoxyethyl)-Modified Antisense Oligonucleotides in Animals and Man. In *Antisense Drug Technology: Principles, Strategies, and Applications, Second Edition*; 2007. https://doi.org/10.1201/9780849387951.ch11.

(16) Gagliardi, M.; Ashizawa, A. T. The Challenges and Strategies of Antisense Oligonucleotide Drug Delivery. *Biomedicines*. 2021. https://doi.org/10.3390/biomedicines9040433.

(17) Sharma, S.; Borski, C.; Hanson, J.; Garcia, M. A.; Link, C. D.; Hoeffer, C.; Chatterjee, A.; Nagpal, P. Identifying Optimal Neuroinflammation Treatment Using Nanoligomer™ Discovery Engine. *ACS Chem. Neurosci.* **2022**, *13* (23), 3247–3256. https://doi.org/10.1021/acschemneuro.2c00365.

(18) Courtney, C. M.; Sharma, S.; Fallgren, C. M.; Weil, M. M.; Chatterjee, A.; Nagpal, P. Reversing Radiation-Induced Immunosuppression Using a New Therapeutic Modality. *Life Sci. Sp. Res.* **2022**, *35*, 127–139. https://doi.org/10.1016/j.lssr.2022.05.002.

(19) McCollum, C. R.; Courtney, C. M.; O'Connor, N. J.; Aunins, T. R.; Jordan, T. X.; Rogers, K. L.; Brindley, S.; Brown, J. M.; Nagpal, P.; Chatterjee, A. Safety and Biodistribution of Nanoligomers Targeting the SARS-CoV-2 Genome for the Treatment of COVID-19. *ACS Biomater. Sci. Eng.* **2023**, *9* (3), 1656–1671. https://doi.org/10.1021/acsbiomaterials.2c00669.

(20) McCollum, C. R.; Courtney, C. M.; O'Connor, N. J.; Aunins, T. R.; Ding, Y.; Jordan, T. X.; Rogers, K. L.; Brindley, S.; Brown, J. M.; Nagpal, P.; Chatterjee, A.; O'Connor, N. J.; Aunins, T. R.; Ding, Y.; Jordan, T. X.; Rogers, K. L.; Brindley, S.; Brown, J. M.; Nagpal, P.; Chatterjee, A. NanoligomersTM Targeting Human MiRNA for Treatment of Severe COVID-19 Are Safe and Nontoxic in Mice. *ACS Biomater. Sci. Eng.* **2022**, *8* (7), 3087–3106. https://doi.org/10.1021/acsbiomaterials.2c00510.

(21) McDonald, J. T.; Enguita, F. J.; Taylor, D.; Griffin, R. J.; Priebe, W.; Emmett, M. R.; Sajadi, M. M.; Harris, A. D.; Clement, J.; Dybas, J. M.; Aykin-Burns, N.; Guarnieri, J. W.; Singh, L. N.; Grabham, P.; Baylin, S. B.; Yousey, A.; Pearson, A. N.; Corry, P. M.; Saravia-Butler, A.; Aunins, T. R.; Sharma, S.; Nagpal, P.; Meydan, C.; Foox, J.; Mozsary, C.; Cerqueira, B.; Zaksas, V.; Singh, U.; Wurtele, E. S.; Costes, S. V.; Davanzo, G. G.; Galeano, D.; Paccanaro, A.; Meinig, S. L.; Hagan, R. S.; Bowman, N. M.; Wallet, S. M.;

Maile, R.; Wolfgang, M. C.; Mock, J. R.; Torres-Castillo, J. L.; Love, M. K.; Lovell, W.; Rice, C.; Mitchem, O.; Burgess, D.; Suggs, J.; Jacobs, J.; Altinok, S.; Sapoval, N.; Treangen, T. J.; Moraes-Vieira, P. M.; Vanderburg, C.; Wallace, D. C.; Schisler, J. C.; Mason, C. E.; Chatterjee, A.; Meller, R.; Beheshti, A.; Bowen, R. A.; Griffin, R. J.; Priebe, W.; Emmett, M. R.; McGrath, M.; Sajadi, M. M.; Harris, A. D.; Clement, J.; Dybas, J. M.; Aykin-Burns, N.; Guarnieri, J. W.; Singh, L. N.; Grabham, P.; Baylin, S. B.; Yousey, A.; Pearson, A. N.; Corry, P. M.; Saravia-Butler, A.; Aunins, T. R.; Nagpal, P.; Meydan, C.; Foox, J.; Mozsary, C.; Cerqueira, B.; Zaksas, V.; Singh, U.; Wurtele, E. S.; Costes, S. V.; Galeano, D.; Paccanaro, A.; Meinig, S. L.; Hagan, R. S.; Bowman, N. M.; Wolfgang, M. C.; Altinok, S.; Sapoval, N.; Treangen, T. J.; Frieman, M.; Vanderburg, C.; Wallace, D. C.; Schisler, J. C.; Mason, C. E.; Chatterjee, A.; Meller, R.; Beheshti, A. Role of MiR-2392 in Driving SARS-CoV-2 Infection. *Cell Rep.* **2021**, *37* (3), 109839. https://doi.org/10.1016/j.celrep.2021.109839.

(22) Risen, S. J.; Boland, S.; Sharma, S.; Weismann, G.; Shirley, P.; Latham, A.; Hay, A. J. D.; Gilberto, V.; Hines, A. D.; Brindley, S.; Brown, J. M.; McGrath, S.; Chatterjee, A.; Nagpal, P.; Moreno, J. A. Targeting Neuroinflammation by Pharmacologic Down-Regulation of Inflammatory Pathways Is Neuroprotective in Protein Misfolding Disorders. *ACS Chem. Neurosci.* **2024**. https://doi.org/10.1101/2022.09.26.509513.

(23) Sharma, S.; Risen, S.; Gilberto, V.; Boland, S.; Chatterjee, A.; Moreno, J.; Nagpal, P. Targeted-Neuroinflammation Mitigation Using Inflammasome-Inhibiting Nanoligomers Is Therapeutic in Experimental Autoimmune Encephalomyelitis (EAE) Mouse Model. *bioRxiv* **2024**. https://doi.org/10.1101/2024.01.11.575262.

(24) Gagliardi, C.; Bunnell, B. A. Large Animal Models of Neurological Disorders for Gene Therapy. *ILAR Journal*. 2009. https://doi.org/10.1093/ilar.50.2.128.

(25) Kilså Jensen, K.; Ørum, H.; Nielsen, P. E.; Nordén, B. Kinetics for Hybridization of Peptide Nucleic Acids (PNA) with DNA and RNA Studied with the BIAcore Technique. *Biochemistry* **1997**. https://doi.org/10.1021/bi9627525.

(26) Fransson, J.; Espander-Jansson, A. Local Tolerance of Subcutaneous Injections. *J. Pharm. Pharmacol.* **1996**, *48* (10). https://doi.org/10.1111/j.2042-7158.1996.tb05892.x.

(27) Reagan□Shaw, S.; Nihal, M.; Ahmad, N. Dose Translation from Animal to Human Studies Revisited. *FASEB J.* **2008**, *22* (3). https://doi.org/10.1096/fj.07-9574lsf.

(28) Zhang, Y.; Huo, M.; Zhou, J.; Xie, S. PKSolver: An Add-in Program for Pharmacokinetic and Pharmacodynamic Data Analysis in Microsoft Excel. *Comput. Methods Programs Biomed.* **2010**, *99* (3). https://doi.org/10.1016/j.cmpb.2010.01.007.

(29) Blanchard, O. L.; Smoliga, J. M. Translating Dosages from Animal Models to Human Clinical Trials-Revisiting Body Surface Area Scaling. *FASEB Journal*. 2015. https://doi.org/10.1096/fj.14-269043.

(30) Larsen, H. J.; Bentin, T.; Nielsen, P. E. Antisense Properties of Peptide Nucleic Acid. *Biochim. Biophys. Acta - Gene Struct. Expr.* **1999**, *1489* (1), 159–166. https://doi.org/10.1016/S0167-4781(99)00145-1.

Supporting Information:

Supplementary Figures:

Sample ID	Below Threshold	p-value
G-CSF (CSF-3)	No	0.570115
IL-10	No	0.876126
IL-3	No	0.795409
LIF	No	0.419316
IL-1 beta	No	0.353403
IL-2	No	0.238137
M-CSF	No	0.899768
IP-10 (CXCL10)	No	0.375312
IL-4	No	0.576022
IL-5	No	0.932894
IL-6	No	0.895916
IL-22	No	0.227429
IL-9	No	0.230025
IL-13	No	0.753696
IL-27	No	0.560482
IL-23	No	0.396848
IFN gamma	No	0.706989
IL-12p70	No	0.252759
GM-CSF	No	0.440844
GRO alpha (CXCL1)	No	0.384355
RANTES (CCL5)	No	0.355962
TNF alpha	No	0.897307
MIP-1 alpha (CCL3)	No	0.799229
MCP-3 (CCL7)	No	0.713972
MCP-1 (CCL2)	No	0.680433
IL-17 A (CTLA-8)	No	0.531265
IL-15	No	0.519355
MIP-2 alpha (CXCL2)	No	0.477553
IL-1 alpha	No	0.540948
ENA-78 (CXCL5)	No	0.820599
Eotaxin (CCL11)	No	0.409270
IL-28	No	0.973117
IL-18	No	0.724024
MIP-1 beta (CCL4)	No	0.788846
IL-31	No	0.413313

Fig. S1. p-values for statistical comparison between NI112 treated and sham-treated animals assessed using blood serum with 36-plex cytokine and chemokine panel, using unpaired t-test for each cytokine.

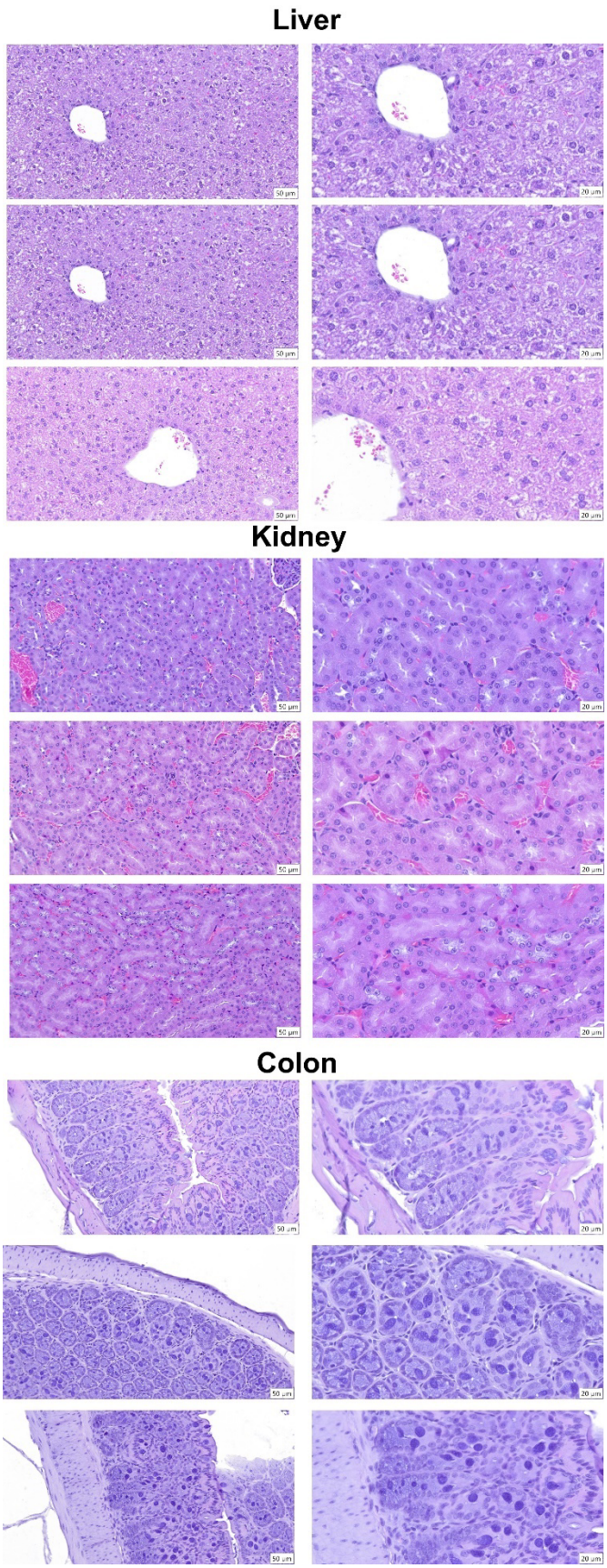

Fig. S2. Additional H&E-stained histology of liver, kidney, and colon samples from mice after long-term (12 weeks) treatment. Histologic findings in each tissue were diagnosed and graded for severity on a 0-5 scale based on inflammation and hemorrhage. 0=absent, 1=minimal (10% of tissue affected), 2=mild (10-25% of tissue affected), 3=moderate (26-50% of tissue affected), 4=marked (51-75% of tissue affected), 5=severe (75% of tissue affected). The middle kidney histology showed mild hemorrhage and was scored at 1. The remaining samples (using further images) were scored as zero, as shown in **Fig. 1B**. There were no significant histologic findings in the liver, kidney, or colons of mice treated with NI112. n=4 animal/group.

Dog Name	ID	DOB	Weight (k	Dose (mg/k	Route	AE Grade - injection	AE Grade - 2hr	AE Grade - 4hr	AE Grade - 8hr	AE Grade - 12hr	AE Grade - 24hr	AE Grade - 48hr	AE Grade - 1 week
Gnocci	4659105	7/3/2021	8.5	75	IV	2	0	0	0	0	0	0	0
Krackle	4490071	10/31/2020	8	75	IV	2	0	0	0	0	0	0	0
Ziti	4686579	8/11/2021	8.8	75	SQ	2	1	1	1	1	1	1	0
Cheddar	4590521	3/29/2021	7.4	5	IV	0	0	0	0	0	0	0	0
Reeses	4490763	10/30/2021	7.7	10	IV	1	0	0	0	0	0	0	0
Brie	4668881	7/17/2021	8.6	15	IV	0	0	0	0	0	0	0	0
George	QZR1	8/26/2021	10.6	15	IV	0	0	0	0	0	0	0	0
Feta	4662939	7/10/2021	6.8	15	IV	0	0	0	0	0	0	0	0
Vaquita	PKO-1	7/7/2021	7.8	45	SQ	1	0	0	0	0	0	0	0
Fin	ROO-1	7/8/2021	7.3	67.5	SQ	1	0	0	0	0	0	0	0
Nougat	4486872	10/23/2020	8.8	67.5	SQ	1	0	0	0	0	0	0	0
Tortellini	4586973	3/26/2021	8.8	67.5	SQ	1	0	0	0	0	0	0	0

VCOG Grading scale	
1	Mild; asymptomatic or mild symptoms, clinical signs or diagnostic observations only; interventions no indicated
2	Moderate; outpatient or non-invasive intervention indicated; moderate limitation of Activities of Daily Living (ADL)
3	Severe or medically significant but not immediately life-threatening; hospitalization or prolonged hospitalization indicated; disabling, significantly limiting ADL
4	Life-threatening consequences; urgent interventions indicated
5	Death related to AE

Fig. S3. (Top) Clinical evaluation data summary for 12 dogs enrolled in the safety-toxicity study, using veterinary cooperative oncology group-common terminology criteria for adverse events (VOG-CTCAE). Adverse events (AE) were documented following API administration and used to determine MTD. The SQ-dosed dogs (IDs PKO-1, ROO-1, 4486872, and 4586973) scored 1 as AE registered mild scratching at the injection site, maximum up to 5-10 minutes. The subjects were fine during the remaining evaluation period (15 minutes) and resumed normal lifestyle. Further, AE evaluations during the day did not observe any changes from normal (scored AE=0 in subsequent examinations). For the above MTD evaluations, dog ID 4659105 showed extreme nausea, loose stool, and vomiting post-injection, but no AE after subsequent evaluations (scored zero). 10 minutes post-injection, subject ID 4490071 had a brief seizure/convulsion lasting 10

seconds and urinated, but then resumed normal function. These two AEs indicated 75 mg/kg dose as above MTD. For SQ, dog ID 4686579 had pain immediately after injection, and the pain reaction lasted 2 minutes, with the injection site painful to touch 5 minutes post-injection. This AE was later traced back to the high pH of SQ injection[26] due to the use of unbuffered saline media to dissolve dried NI112 powder. However, as per IACUC protocol at CSU, the AE resulted in 75mg/kg marked as above MTD. As seen in subsequent CBC/chemistry, and clinical evaluations, no organ damage or pathological events were seen at the highest 75 mg/kg dosages (**Fig. 1C-F**, **S4, S5**).

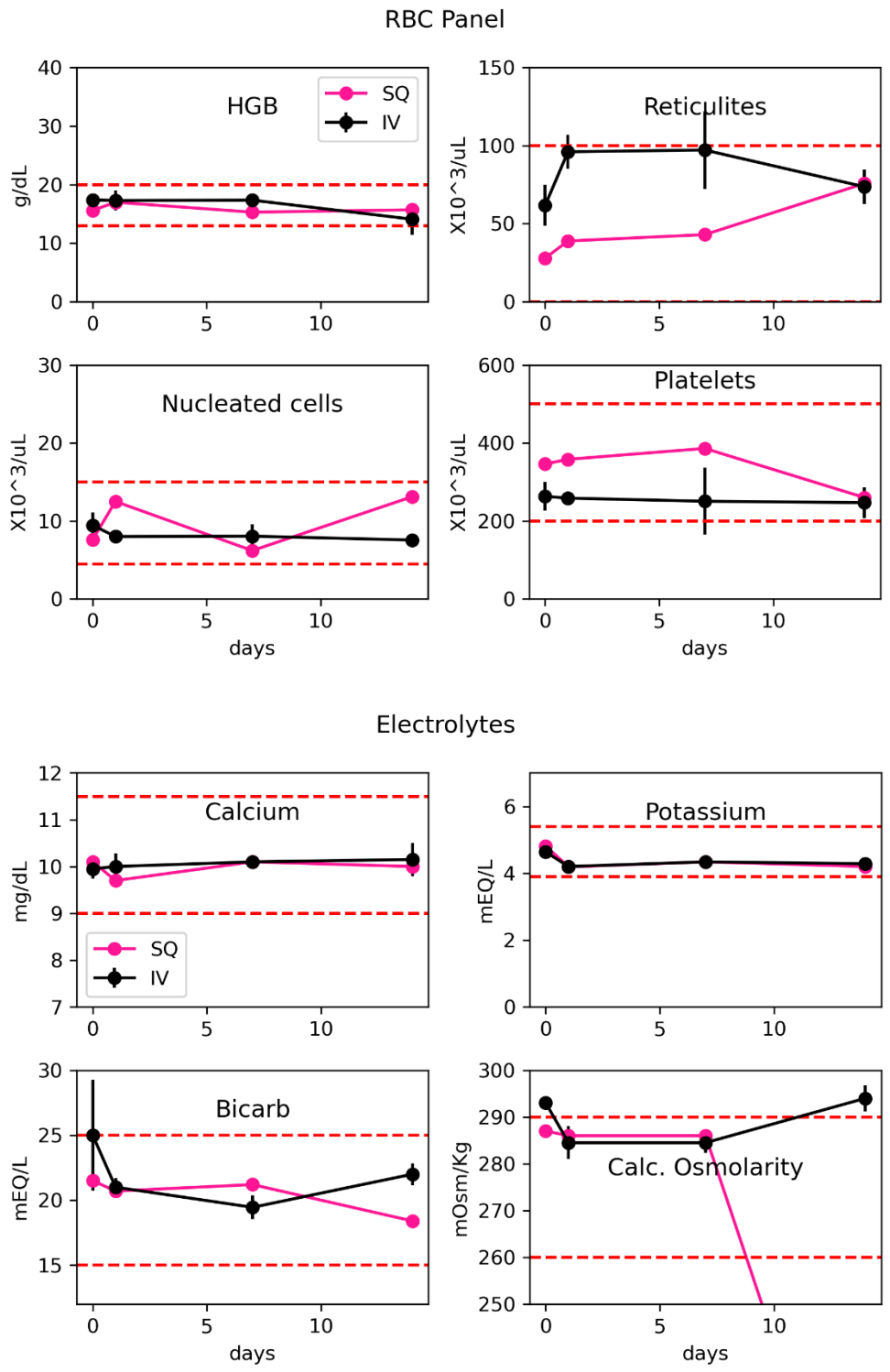

Fig. S4. Monitoring health using Red Blood Cells (RBC) panel (Top) and Electrolyte panel (Bottom). RBC panel includes Hemoglobin (HGB), reticulocyte nucleated cells, and platelets, whereas the Electrolyte panel includes calcium, potassium, bicarbonate, and calc. osmolarity, with extensive CBC/chemistry monitoring over 14 days using three clinically translatable routes of drug administration (intravenous IV black, subcutaneous SQ pink), after administration of the

highest dose (75 mg/kg dose IV and SQ) well above MTD. The red dashed lines show upper and lower normal limits for each measurement. The curves show mean values, and the bars show standard deviation (Mean ± SD).

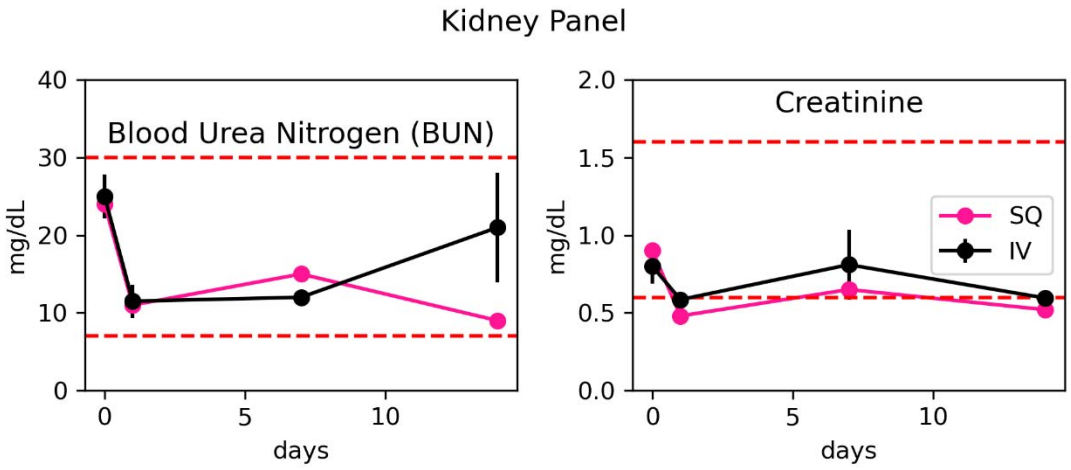

Fig. S5. Monitoring kidney health using blood urea nitrogen, and creatinine, as seen using extensive CBC/chemistry monitoring over 14 days using three clinically translatable routes of drug administration (intravenous IV black, subcutaneous SQ pink), after administration of the highest dose (75 mg/kg dose IV and SQ) well above MTD. The red dashed lines show upper and lower normal limits for each measurement. The curves show mean values, and the bars show standard deviation (Mean ± SD).

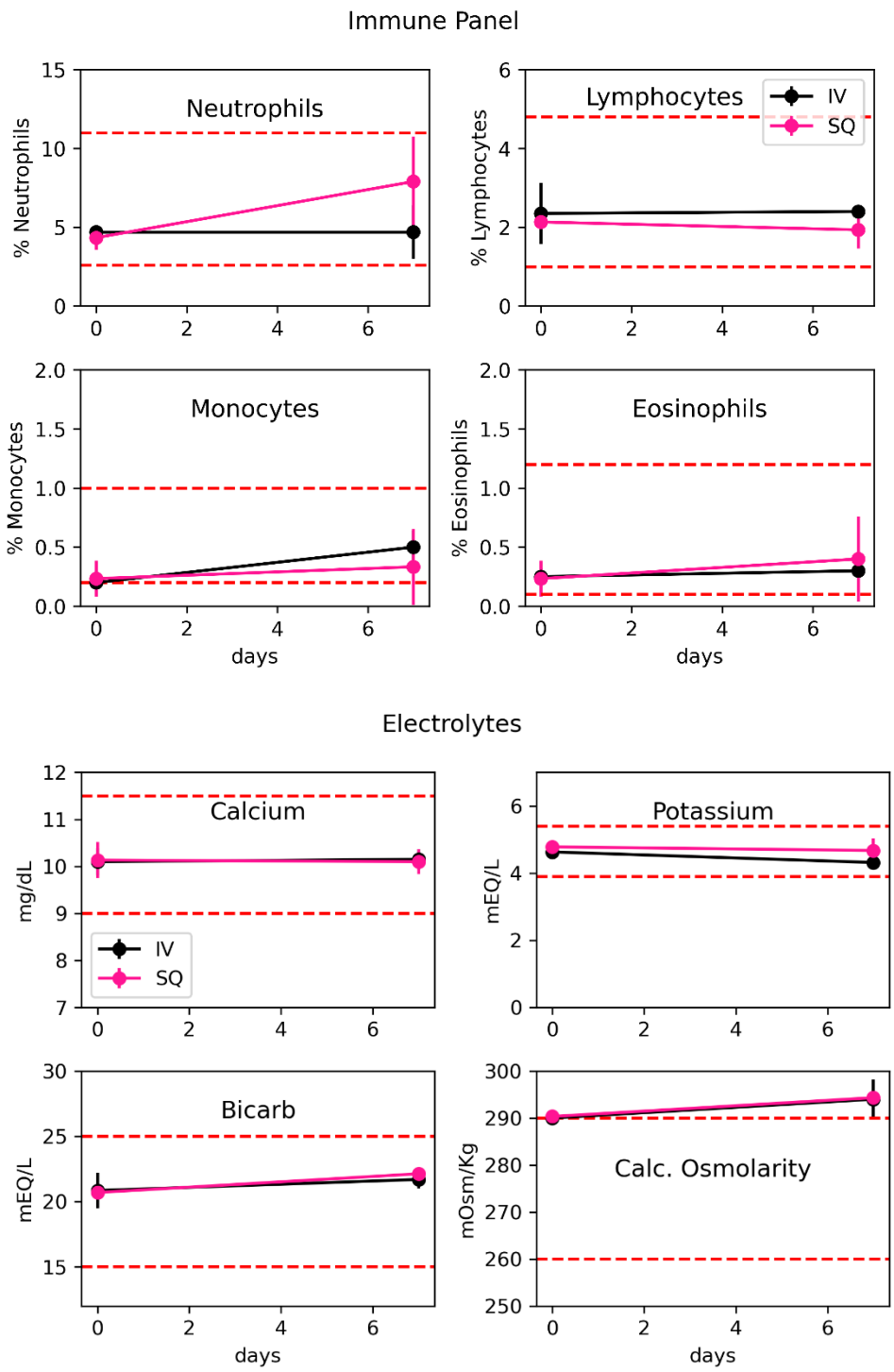

Fig. S6. Lack of any immunogenic response, or imbalance in electrolyte concentrations can be seen using extensive CBC/chemistry monitoring over 7 days after administration of 15 mg/kg and 67.5 mg/kg MTD dosing using IV and SQ routes, respectively. The red dashed lines show upper and lower normal limits for each measurement. Using monitoring of different immune

components and total blood count, all immune biomarkers were found to be normal. The curves show mean values, and the bars show standard deviation (Mean ± SD).

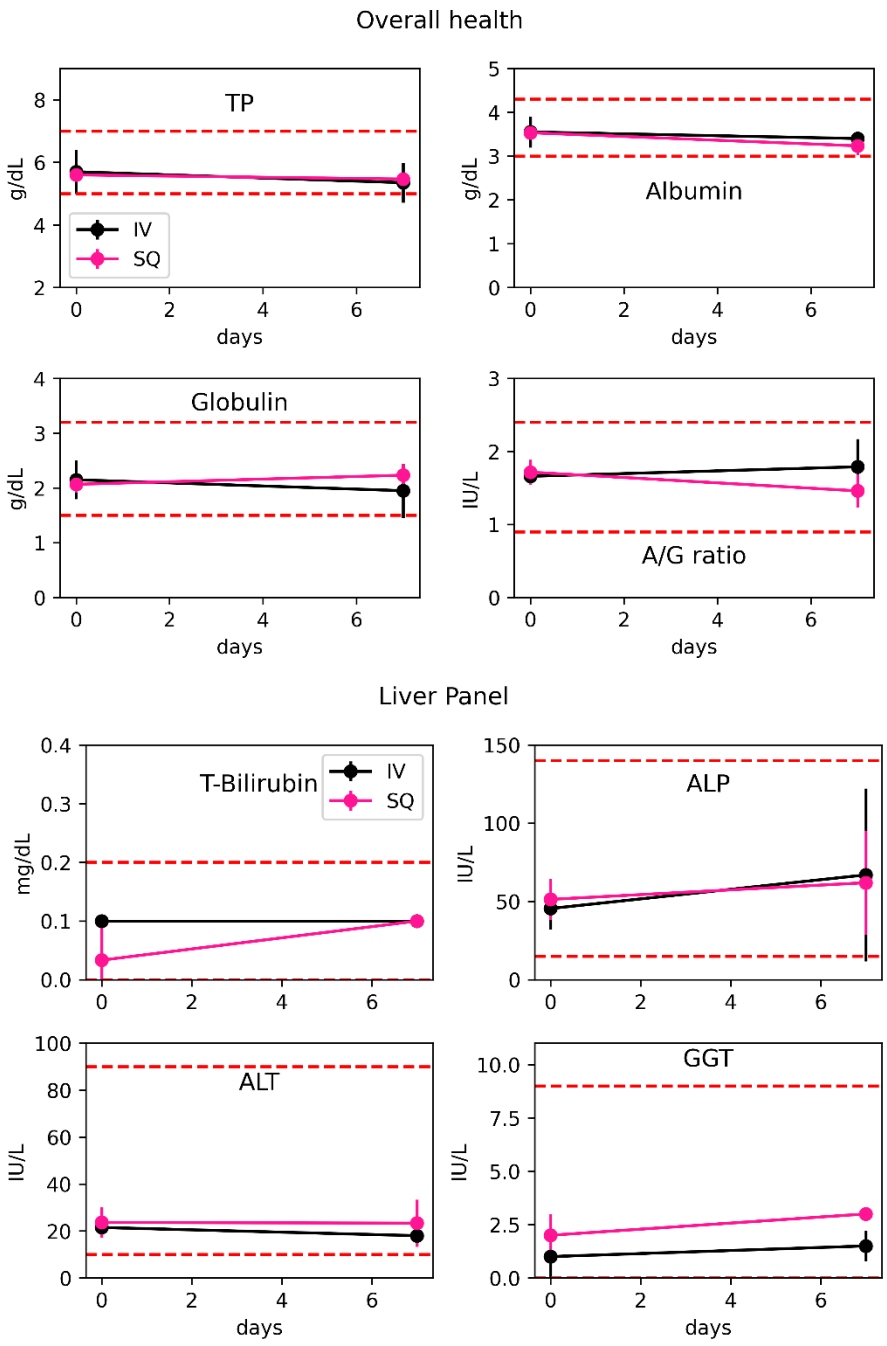

Fig. S7. Lack of any adverse impact on the overall health (using total protein (TP), albumin, globulin, Albumin, and A/G ratio), or liver health (using total bilirubin, ALP), ALT, and GGT enzymes), can be seen using extensive CBC/chemistry monitoring over 7 days after administration of 15 mg/kg and 67.5 mg/kg MTD dosing using IV and SQ routes, respectively. The red dashed lines show upper and lower normal limits for each measurement. The curves show mean values, and the bars show standard deviation (Mean ± SD).

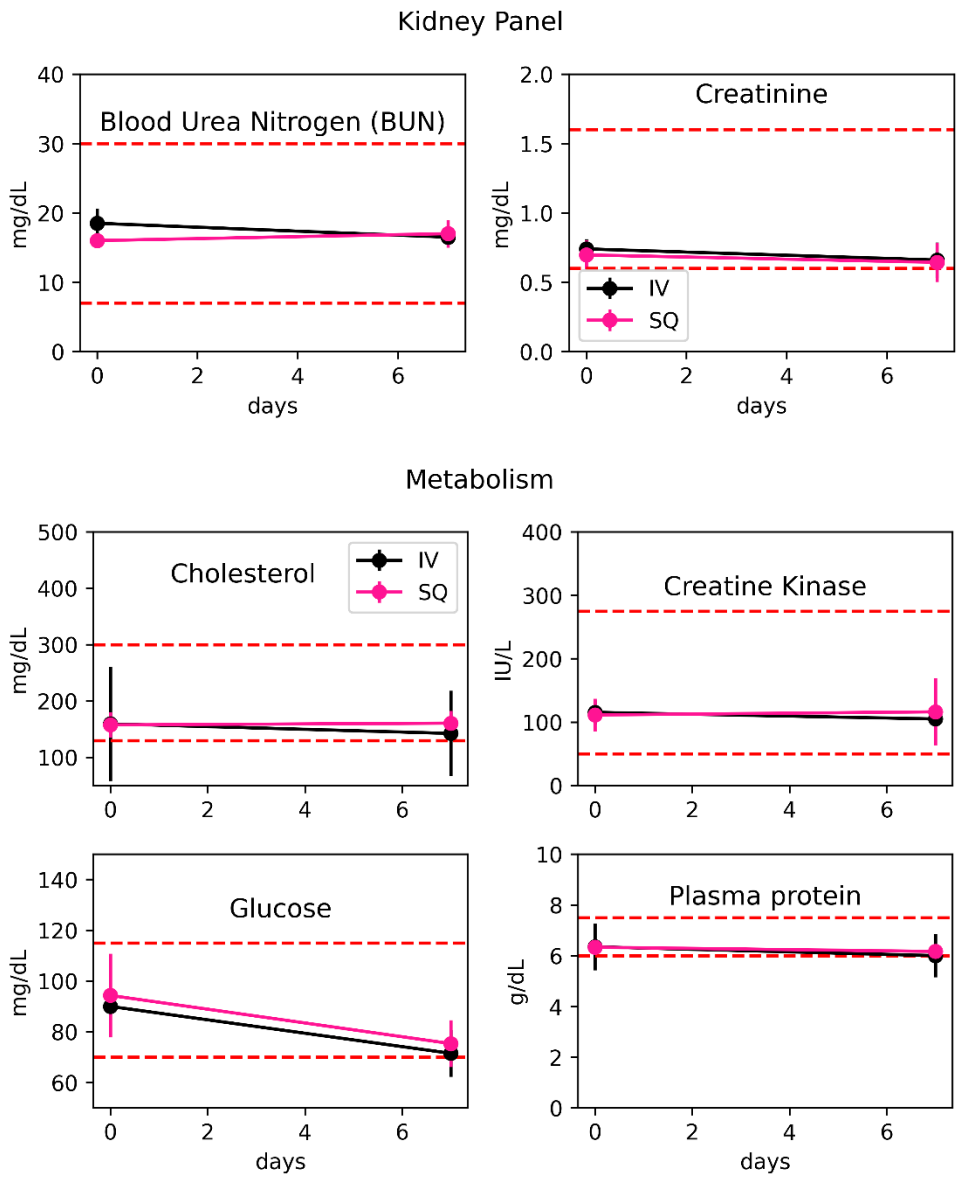

Fig. S8. Lack of any adverse changes in kidney health (using blood urea nitrogen, and creatinine), and metabolism and cardiac health (using cholesterol, creatinine kinase, glucose, and plasma protein), can be seen using extensive CBC/chemistry monitoring over 7 days after administration of 15 mg/kg and 67.5 mg/kg MTD dosing using IV and SQ routes, respectively. The red dashed lines show upper and lower normal limits for each measurement. The curves show mean values, and the bars show standard deviation (Mean ± SD).

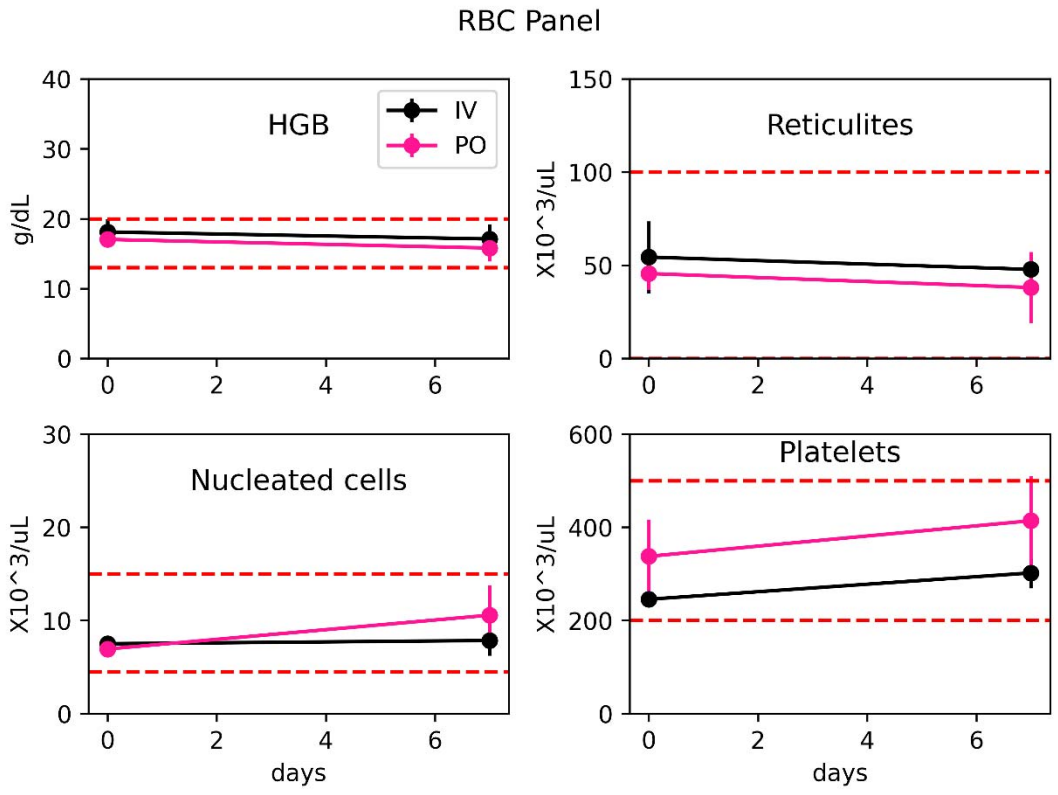

Fig. S9. Lack of any adverse changes in the RBC panel (Hemoglobin (HGB), reticulates, nucleated cells, and platelets) can be seen using extensive CBC/chemistry monitoring over 7 days after administration of 15 mg/kg and 67.5 mg/kg MTD dosing using IV and SQ routes, respectively. The red dashed lines show upper and lower normal limits for each measurement. The curves show mean values, and the bars show standard deviation (Mean ± SD).

PKSolver 2.0 *Non-Compartmental Analysis of Plasma Data after Intravenous Bolus Input*

Time Unit	h	Method	Linear up/Log down
Conc Unit	nmol/L	Analyst	Sachi Bio
Dose	133	Date	2023-11-14
Dose Unit	nmol	Time	16:36:24

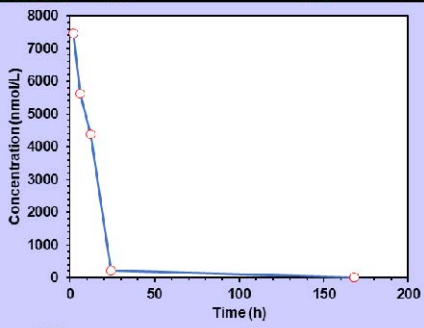

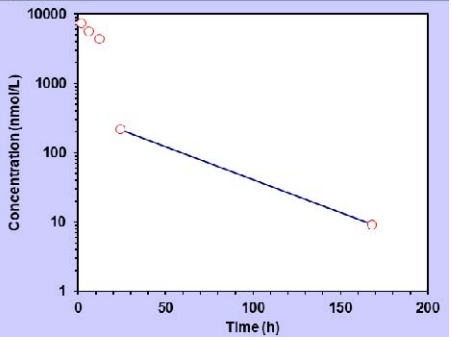

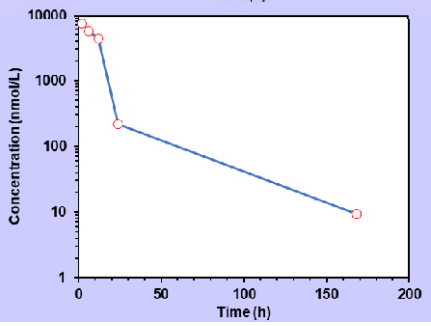

PKSolver 2.0 *Non-Compartmental Analysis of Plasma Data after Extravascular Input*

Time Unit	h	Method	Linear up/Log down
Conc Unit	nmol/L	Analyst	Sachi Bioworks
Dose	633	Date	2023-11-14

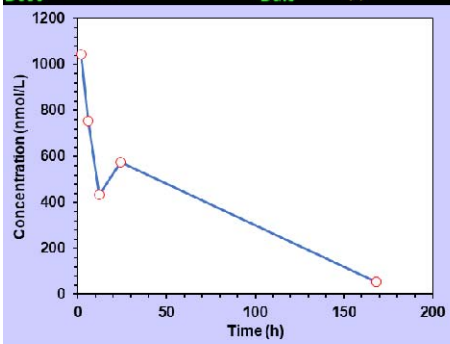

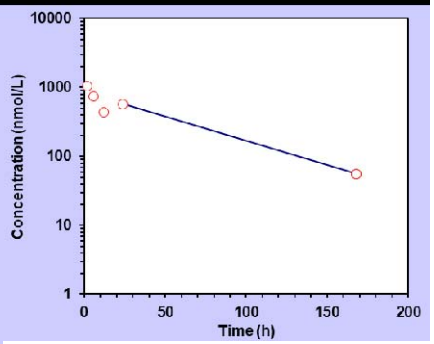

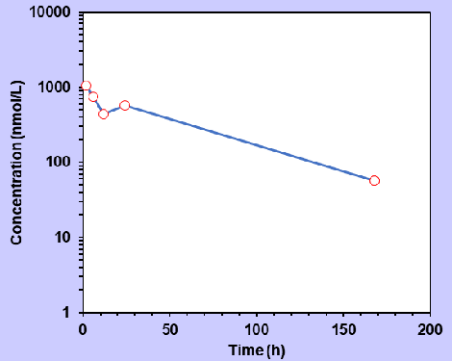

Fig. S10. **Pharmacokinetic modeling** using PK Solver[28] for mice using the IV route (Top) and SQ route (bottom) of administration. n=4 mice per group, Median ± SE was used for analysis (**Fig.2**).

Blood Serum

Parameter	Unit	IV-Value
Lambda_z	1/h	0.02188664
t1/2	h	31.66987628
Tmax	h	2
Cmax	nmol/L	7465.434636
C0	nmol/L	8607.189284
Clast_obs/Cmax		0.001236867
AUC 0-t	nmol/L*h	97870.60687
AUC 0-inf_obs	nmol/L*h	98292.49667
AUC 0-t/0-inf_obs		0.995707813
AUMC 0-inf_obs	nmol/L*h^2	1323877.909
MRT 0-inf_obs	h	13.46875859
Vz_obs	(nmol)/(nmol/L)	0.0618233
Cl_obs	(nmol)/(nmol/L)/h	0.001353104
Vss_obs	(nmol)/(nmol/L)	0.018224635

Parameter	Unit	SQ	IP	IN
Lambda_z	1/h	0.016123265	0.007100186	0.014764401
t1/2	h	42.99049633	97.62380894	46.94719377
Tmax	h	2	6	6
Cmax	nmol/L	1043.818156	6943.677994	2188.883422
Tlag	h	0	0	0
Clast_obs/Cmax		0.054112586	0.026453227	0.005786375
AUC 0-t	nmol/L*h	46355.83109	298853.9706	121978.5632
AUC 0-inf_obs	nmol/L*h	49859.07307	324724.095	122836.4172
AUC 0-t/0-inf_obs		0.929737122	0.920331984	0.993016289
AUMC 0-inf_obs	nmol/L*h^2	3232580.765	40069732.76	8350160.182
MRT 0-inf_obs	h	64.83435344	123.3962413	67.97788776
Vz/F_obs	(nmol)/(nmol/L)	0.78742012	0.289295452	0.367775564
Cl/F_obs	(nmol)/(nmol/L)/h	0.012695784	0.002054051	0.005429986

Brain

Parameter	Unit	IV-Value
Lambda_z	1/h	0.003510262
t1/2	h	197.4630693
Tmax	h	12
Cmax	nmol/L	61.03082285
C0	nmol/L	44.81459984
Clast_obs/Cmax		0.243221364
AUC 0-t	nmol/L*h	3878.800019
AUC 0-inf_obs	nmol/L*h	8107.543759
AUC 0-t/0-inf_obs		0.478418635
AUMC 0-inf_obs	nmol/L*h^2	2177628.907
MRT 0-inf_obs	h	268.5929267
Vz_obs	(nmol)/(nmol/L)	4.673290321
Cl_obs	(nmol)/(nmol/L)/h	0.016404475
Vss_obs	(nmol)/(nmol/L)	4.406125988

Parameter	Unit	SQ	IP	IN
Lambda_z	1/h	0.002612877	0.001607731	0.006629279
t1/2	h	265.2812381	431.1337428	104.5584552
Tmax	h	2	24	6
Cmax	nmol/L	199.705955	60.95337791	48.678838
Tlag	h	0	0	0
Clast_obs/Cmax		0.440565731	0.605544783	0.075776254
AUC 0-t	nmol/L*h	18917.76333	15999.71625	4677.87644
AUC 0-inf_obs	nmol/L*h	52590.84026	38957.5337	5234.301951
AUC 0-t/0-inf_obs		0.359715936	0.410696333	0.893696329
AUMC 0-inf_obs	nmol/L*h^2	19993811.87	24507547.97	780364.1981
MRT 0-inf_obs	h	380.1766957	629.0836623	149.0904051
Vz/F_obs	(nmol)/(nmol/L)	4.606538179	10.64929682	19.22209675
Cl/F_obs	(nmol)/(nmol/L)/h	0.012036317	0.017121207	0.127428644

Fig. S11. **Pharmacokinetic modeling parameters** obtained using PK Solver[28] for mice using IV (n=4/group), SQ (n=4/group), IP (n=6/group), and IN (n=6/group) in (Top) blood serum; and (Bottom) brain tissue. Median ± SE used for average and SE analysis shown in **Figs.2, 3, 4**.

Parameter	Unit	IV_75-1	IV_75-2	IV_15-1	IV_15-2	IV_15-3
Lambda_z	1/h	0.006033929	0.007969055	0.011073126	0.011282599	0.015384035
t1/2	h	114.8749339	86.97985051	62.59724594	61.43506382	45.05626686
Tmax	h	4	8	2	4	2
Cmax	nmol/L	6652.596265	10882.5493	6009.853813	4327.951134	4046.45278
C0	nmol/L	4.020552635	4.352701995	1.301984552	26.80893082	210.9260819
Clast_obs/Cmax		0.142660093	0.055446567	0.081090159	0.139534847	0.078026365
AUC 0-t	nmol/L*h	823878.4461	947476.0922	234234.8857	279828.9419	226942.7149
AUC 0-inf_obs	nmol/L*h	981165.683	1023193.982	278245.9453	333353.844	247465.9393
AUC 0-t/0-inf_obs		0.8396935	0.9259985	0.841826771	0.839435173	0.917066468
AUMC 0-inf_obs	nmol/L*h^2	188082085.5	135530645.5	25127323.17	31361883.42	17453924.73
MRT 0-inf_obs	h	191.6924825	132.4584075	90.30616113	94.07986134	70.53061435
Vz_obs	(µmol)/(nmol/L)	0.008445541	0.006132043	0.003245644	0.002658798	0.002626723
Cl_obs	(µmol)/(nmol/L)/h	5.09598E-05	4.88666E-05	3.59394E-05	2.99982E-05	4.04096E-05
Vss_obs	(µmol)/(nmol/L)	0.009768609	0.006472791	0.003245552	0.002822222	0.002850114

Parameter	Unit	SQ_67-1	SQ_67-2	SQ_67-3
Lambda_z	1/h	0.00201432	0.002269343	0.00896967
t1/2	h	344.1097602	305.4395491	77.27677534
Tmax	h	2	8	12
Cmax	nmol/L	4778.586227	5508.249334	10452.3427
Tlag	h	0	0	0
Clast_obs/Cmax		0.36532981	0.340108081	0.12321544
AUC 0-t	nmol/L*h	372417.7367	440322.8461	543873.0556
AUC 0-inf_obs	nmol/L*h	1239092.336	1265848.027	687455.8169
AUC 0-t/0-inf_obs		0.300556888	0.347848112	0.791138924
AUMC 0-inf_obs	nmol/L*h^2	604018644.9	533897381.2	73132513.37
MRT 0-inf_obs	h	487.4686312	421.7705206	106.3814016
Vz/F_obs	(µmol)/(nmol/L)	0.018029363	0.015665013	0.007297788
Cl/F_obs	(µmol)/(nmol/L)/h	3.63169E-05	3.55493E-05	6.54588E-05

Fig. S12. **Pharmacokinetic modeling parameters** obtained using PK Solver[28] for dogs using IV MTD (15 mg/kg), IV acute dose (75 mg/kg, 5x MTD), and SQ (67.5 mg/kg).

TOC IMAGE:

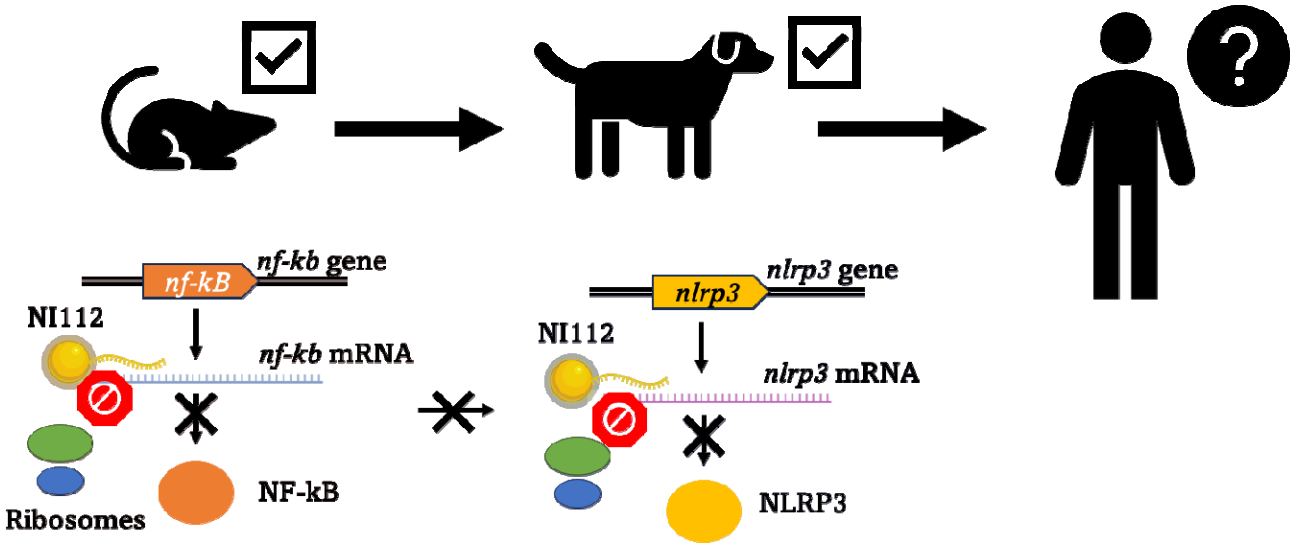
nf-kB
nf-kb gene
NI112
nf-kb mRNA
Ribosomes
NF-kB
nlrp3
nlrp3 gene
NI112
nlrp3 mRNA
NLRP3